The Journal of Neuroscience, November 1994, 14(11): 6667–6686

Cellular and Molecular Characterization of Ca^{2+} Currents in Acutely Isolated, Adult Rat Neostriatal Neurons

Jose Bargas,[1] Angela Howe,[2] James Eberwine,[3] Y. Cao,[3] and D. James Surmeier[2]

[1]Instituto de Fisologia Celular, Universidad Nacional Autonoma de Mexico, 04510 Mexico, [2]Department of Anatomy and Neurobiology, College of Medicine, University of Tennessee, Memphis, Tennessee 38163, and [3]Department of Pharmacology, University of Pennsylvania, Philadelphia, Pennsylvania 19104

Ca^{2+} currents in acutely isolated, adult rat neostriatal neurons were studied with whole-cell voltage-clamp techniques. In the vast majority of neurons (~90%, $n > 250$), currents were exclusively of the high-voltage-activated (HVA) type. HVA currents activated near −40 mV and reached their maximum amplitude near 0 mV. Quasi-steady-state inactivation curves in many neurons were well fitted only with a sum of Boltzmann functions, suggesting that the HVA currents were heterogeneous. Although the block of whole-cell current by Cd^{2+} was well fitted with a single isotherm having an IC_{50} of near 1 μM, experiments with organic channel antagonists suggested that at least four types of HVA channels were expressed by most cells. On average, the L-channel antagonist nifedipine (5–10 μM) blocked 31 ± 10% of the whole-cell current ($n = 20$), the N-channel antagonist ω-conotoxin GVIA (ω-CgTx) (2–5 μM) blocked 27 ± 11% ($n = 20$), and the P-channel antagonist ω-agatoxin IVA (100–500 nM) blocked 21 ± 10% ($n = 18$). In many neurons, the block by ω-CgTx was partially or completely reversible. In cells tested with a combination of these antagonists, 34 ± 17% of the peak Ca^{2+} current remained unblocked ($n = 13$). Single-cell expression profiling of medium-sized neurons revealed the presence of rbA and rbB Ca^{2+} channel α1 subunit mRNAs but low or undetectable levels of rbC mRNA ($n = 12$). These findings suggest that although adult neostriatal projection neurons do not express significant levels of LVA Ca^{2+} current, they do express a pharmacologically and structurally heterogeneous population of HVA currents.

[Key words: Ca^{2+} current, neostriatum, dihydropyridine, ω-conotoxin GVIA, ω-agatoxin IVA, voltage clamp, mRNA profiling]

Ca^{2+} entry into neurons through voltage-dependent channels is of broad functional significance (Rasmussen and Barrett, 1984; Miller, 1987, 1988; Hosey and Lazdunski, 1988). Transmembrane current carried by Ca^{2+} ions influences spike generation and the patterning of discharge directly by altering transmembrane potential and indirectly by promoting the opening of Ca^{2+}-dependent channels (e.g., Lancaster et al., 1991; McCobb and Beam, 1991). Elevations in cytosolic Ca^{2+} concentration subsequent to activation of voltage-dependent channels are also thought to stimulate a broad spectrum of intracellular signaling enzymes, including those involved in transmitter release, receptor sensitivity, and gene expression (Rasmussen and Barrett, 1984; Augustine et al., 1987; Miller, 1987, 1988; Holliday et al., 1991; Llano et al., 1991; Murphy et al., 1991).

Biophysical and pharmacological studies of neuronal Ca^{2+} currents commonly have divided channels into low-voltage-activated (LVA) and high-voltage-activated (HVA) categories (Tsien et al., 1988, 1991; Bean, 1989; Carbone and Swandulla, 1989; Kostyuk, 1989). LVA, or T-type, currents are activated at relatively hyperpolarized potentials and inactivate rapidly. HVA currents, which are activated at relatively depolarized membrane potentials, are heterogeneous (Tsien et al., 1991). Pharmacological studies of mammalian brain neurons have identified three types of HVA current—L, N, and P. Although the biophysical differences between these currents are modest in most cells, there are differences in their subcellular distribution and coupling to receptor-mediated signaling pathways (e.g., Westenbroek et al., 1990; Muller and Connor, 1991; Beech et al., 1992).

Microelectrode recordings of medium spiny neostriatal neurons in tissue slices have shown that Ca^{2+} currents are important in spike generation and patterning (Kita et al., 1985; Galarraga et al., 1989; Pineda et al., 1992). HVA, rather than LVA, currents appear to subserve these functions in adult medium spiny neurons as they do not exhibit properties—such as bursting or pacemaking—that are typically found in neurons with prominent LVA Ca^{2+} currents (Llinas, 1988). This inference is at odds with a recent patch-clamp study showing that a large proportion of adult neostriatal neurons express prominent LVA currents (Hoehn et al., 1993). This study also found that L-type HVA currents do not contribute substantively to whole-cell currents, in contrast to previous reports (Kita et al., 1985; Cherubini and Lanfumey, 1987).

The basis for the apparent discrepancy is unclear. One possibility is that projection (medium spiny) and interneuronal cell types differ in their expression of Ca^{2+} channel types and the sample of Hoehn et al. (1993) was biased toward interneurons. Recent work with striatal interneurons in slices by Kawaguchi (1993) supports this inference. In this study, we have attempted to address this question directly by working exclusively with either retrogradely labeled projection neurons or neurons with

Received Sept. 27, 1993; revised Apr. 25, 1994; accepted May 5, 1994.

We thank Dr. T. Snutch for the Ca^{2+} channel cDNAs, Dr. C. J. Wilson for rhodamine bead injections, Dr. L. Dudkin for her technical help, P. Mermelstein for participating in some of the later biophysical experiments, and Drs. B. Foehring, K. Mackie, J. Harrington, and R. Scroggs for critically reading the manuscript. This work was supported by USPHS Grants NS 28889 and NS 26473 to D.J.S., NS23886 to J.E., and MH-10400 to A.H.

Correspondence should be addressed to Dr. James Surmeier at the above address.

similar morphology. In this restricted population, Ca^{2+} currents were found to be of the HVA type, in agreement with previous slice studies. To provide structural information about the channel types underlying these currents, single-cell mRNA expression profiling was performed to determine whether mRNA from one or more of the cloned HVA gene families could be detected in individual neurons subjected biophysical analysis.

Materials and Methods

Acute-dissociation procedure. Neostriatal neurons from adult (>4 weeks) rats were acutely dissociated using procedures similar to those we have previously described (Surmeier et al., 1991, 1992). In brief, rats were anesthetized with methoxyflurane and decapitated; brains were quickly removed, iced and then blocked for slicing. The blocked tissue was cut in 400 μm slices with a Vibroslice (Campden Instruments, London, England) while bathed in a low-Ca^{2+} (100 μM), *N*-[2-hydroxyethyl]piperazine-*N*-[2-ethanesulfonic acid] (HEPES)-buffered salt solution (in mM: 140 Na isethionate, 2 KCl, 4 $MgCl_2$, 0.1 $CaCl_2$, 23 glucose, 15 HEPES, pH = 7.4, 300–305 mOsm/liter). Slices were then incubated for 1–6 hr at room temperature (20–22°C) in a $NaHCO_3$-buffered saline bubbled with 95% O_2, 5% CO_2 (in mM: 126 NaCl, 2.5 KCl, 2 $CaCl_2$, 2 $MgCl_2$, 26 $NaHCO_3$, 1.25 NaH_2PO_4, 1 pyruvic acid, 10 glucose, pH = 7.4 with NaOH, 300–305 mOsm/liter); in later experiments reduced glutathione (100 μM) or ascorbic acid (100 μM) was added to the holding solutions. Slices were then removed into the low-Ca^{2+} buffer and, with the aid of a dissecting microscope, regions of the dorsal neostriatum were dissected and placed in an oxygenated Cell-Stir chamber (Wheaton, Inc.) containing pronase (1–3 mg/ml) in HEPES-buffered Hanks' balanced salt solution (HBSS; Sigma Chemical Co., St. Louis, MO) at 35°C. Dissections were limited to tissue rostral to the anterior commissure to reduce the possibility of contamination from pallidum. Although pronase treatment provided the highest yield of viable cells (all of the data shown in the figures was taken from pronase treated neurons), other enzymes such as papain and trypsin were tried with comparable results. After 20–30 min of enzyme digestion, tissue was rinsed three times in the low-Ca^{2+}, HEPES-buffered saline and mechanically dissociated with a graded series of fire-polished Pasteur pipettes. The cell suspension (2 ml) was then plated into a 35 mm Lux petri dish mounted on the stage of an inverted microscope containing 1 ml of HEPES-buffered HBSS. After allowing the cells to settle, the solution bathing the cells was changed to our normal recording external solution.

Whole-cell recordings. Whole-cell recordings employed standard techniques (Hamill et al., 1981; Surmeier et al., 1992). Electrodes were pulled from Corning 7052 glass and fire-polished prior to use. In some experiments, electrodes were coated with Sylgard. The internal solution consisted of (in mM) 180 *N*-methyl-D-glucamine (NMG), 40 HEPES, 4 $MgCl_2$, 0–10 EGTA or 0.1 BAPTA, 12 phosphocreatine, 2 Na_2ATP, 0.2 Na_3GTP, 0.1 leupeptin, pH = 7.2–7.3 with H_3PO_4 or CH_3SO_3H, 265–270 mOsm/liter (no differences in physiology were observed between acids). In some experiments, NMG was replaced with Tris without altering current properties in any noticeable way (cf. Malecot et al., 1988). All of the data presented was gathered using the standard NMG internal (neutralized with H_3PO_4). The pH of NMG solutions was measured with a Corning model 476570 probe. The external solution consisted of (in mM) 135 NaCl, 20 CsCl, 1 $MgCl_2$, 10 HEPES, 0.001 TTX, 2–10 $CaCl_2$ or $BaCl_2$, 10 glucose, pH = 7.3 with NaOH, 300–305 mOsm/liter; in some experiments, TEA Cl was used instead of NaCl as the major external salt. In experiments where higher concentrations of Ba^{2+} or Ca^{2+} were used, the Mg^{2+} concentration was fixed at 1 mM and the osmolarity was adjusted to 300–305 mOsm/liter with glucose. Nifedipine and (±)Bay K 8644 (Research Biochemicals Inc., Natick, MA) were made up as concentrated stocks in 95% ethanol and then diluted immediately before use. These solutions were protected from ambient light. Final ethanol concentrations never exceeded 0.05%. Although previous experiments had shown that this concentration had no effect on currents, ethanol controls were run for every cell. ω-Conotoxin GVIA (ω-CgTx) (Peninsula Lab., Belmont, CA; Research Biochemicals Inc., Calbiochem, San Diego, CA) was made up as a concentrated stock in water, aliquoted, and frozen. ω-Agatoxin IVA (ω-AgTx) (Peptides International, Louisville, KY) was made up as a concentrated stock, aliquoted, and frozen; final dilution were made in external media containing 0.01% cytochrome C. This concentration of cytochrome C was used because 0.1% (Mintz et al., 1992) had effects of its own on our currents, and dose–response experiments with ω-AgTx suggested that 0.01% (0.1 mg/ml) was a sufficient carrier concentration with our perfusion tubing (largely Teflon). More recent work using this toxin (Sather et al., 1993) has also reported using this lower cytochrome C concentration without loss of activity.

Electrode resistances were typically 3–6 MΩ in the bath. Recordings were obtained with an Axon Instruments 200 patch-clamp amplifier and controlled and monitored with a PC 486 clone running PCLAMP (ver. 5.0–5.5) with a 125 kHz interface (Axon Instruments, Inc., Foster City, CA). After seal rupture, series resistance (7–15 MΩ) was compensated (70–80%) and periodically monitored. Because whole-cell currents never exceeded 2 nA (usually <600 pA), errors in voltage due to inadequate compensation should never have exceeded a few millivolts. Recordings were made only from medium-sized neurons (6–12 μm somal diameter) that had only a few short (<50 μm) proximal dendrites. The adequacy of voltage control was assessed after compensation by examining the tail currents generated by strong depolarizations. Cells in which tail currents did not decay rapidly and smoothly at subthreshold potentials were discarded. Drugs were applied with a gravity-fed "sewer pipe" system. The array of application capillaries (~150 μm i.d.) was positioned a few hundred micrometers from the cell under study. Solution changes were effected by a altering the position of the array with a DC drive system controlled by a microprocessor-based controller (Newport-Klinger, Inc., Irvine, CA). Solution changes were complete within 1–2 sec. Potentials were not corrected for the liquid junction potential with the NMG-PO_4 internal solution, which was estimated to be 7 mV.

Statistical analyses (including non-linear curve fitting) were performed with SYSTAT (ver. 5, SYSTAT, Inc., Evanston, IL). Sample statistics are given either as means with standard deviations or as medians. Box plots were used for graphic presentation of the data because of the small sample sizes (Tukey, 1977). The box plot represents the distribution as a box with the median as a central line and the hinges as the edges of the box (the hinges divide the upper and lower halves of the distributions in half). The inner fences (shown as a line originating from the edges of the box) run to the limits of the distribution excluding outliers (defined as points that are more than 1.5 times the interquartile range beyond the inner fence; Tukey, 1977); outliers are shown as asterisks or circles.

Data were gathered using either a combination of voltage steps or ramps. In most situations, those currents not blocked by Cd^{2+} (200–400 μM) were subtracted from control records (in nearly all cells, there was little or no evidence for Cd^{2+}-insensitive currents at membrane potentials below 0 mV; above this potential, small tail currents that were sensitive to Cl^- replacement were seen). Peak current–voltage plots derived from Ca^{2+} or Ba^{2+} currents evoked with short (10–30 msec) step protocols (Fig. 1*A*) and from slow voltage ramps (0.25–1.0 mV/msec) (Fig. 1*B*) were very similar in most cells in which they were compared (n = 10 of 11); the comparison in an exemplary neuron is shown in Figure 1*B*. Faster ramps yielded current–voltage curves that were shifted toward more depolarized potentials. Using the Goldman-Hodgkin-Katz constant current equation (Kay and Wong, 1987; Hille, 1992), an estimate of membrane permeability as a function of membrane voltage was computed from the relationship

$$I(V_m) = \gamma(V_m) \cdot P(V_m);$$

where

$$\gamma(V_m) = z^2\left(\frac{V_m F^2}{RT}\right)\left(\frac{[\mathrm{Ca}]_i - [\mathrm{Ca}]_o \exp\left(-\frac{zV_mF}{RT}\right)}{1 - \exp\left(-\frac{zV_mF}{RT}\right)}\right), \quad (1)$$

where $I(V_m)$ = measured transmembrane current, V_m = membrane potential (mV), z = 2, F = 9.648 × 10^4 C mol^{-1}, R = 8.315 V C K^{-1} mol^{-1}, T = 273.16 + 20°K, $[Ca]_i$ = nominally 10 nM, $[Ca]_o$ = 2–10 mM, and $P(V_m)$ = membrane permeability to Ca^{2+} or Ba^{2+} as a function of membrane potential. It should be noted that the units of $I(V_m)$ are those of current density (A/cm^2). Because we did not measure membrane surface area, all currents were normalized by our estimate of the modal surface area based upon whole-cell capacitance; the modal capacitance was 8 pF, yielding an estimated surface area of 8.0 × 10^{-6} cm^2 assuming 1 μF/cm^2. Although inexact, our estimates should be within a factor of 1.5 of the true values based upon variation in the somal diameters of medium-sized neurons.

Over the potential range where the driving force term from Equation

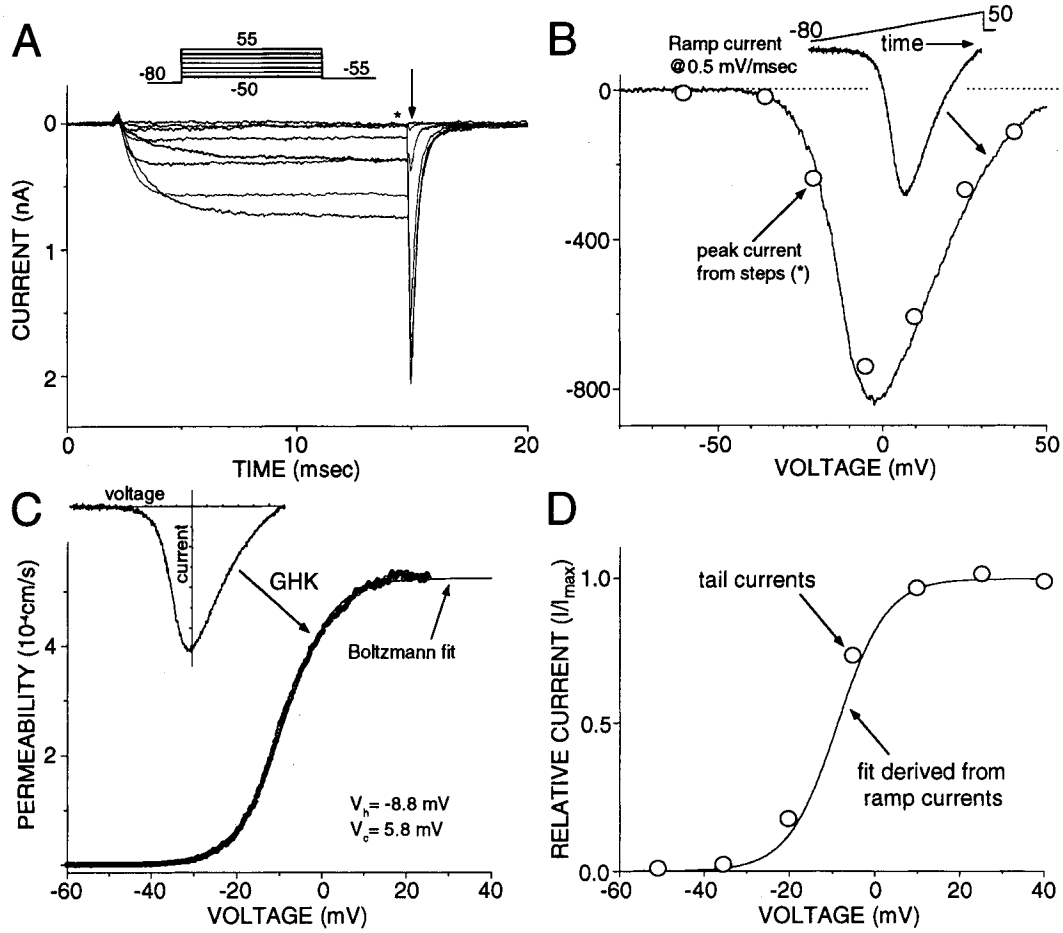

Figure 1. Current activation by step voltage commands and ramps. *A*, Inward currents elicited from a −80 mV holding potential and commands from −55 to +55 mV with 15 mV steps (see stimulation protocol on *inset* at *top*). *B*, Inward current obtained after a ramp depolarization (*inset*) of 0.5 mV/msec. After leak subtraction, *I–V* plots were constructed with both peak currents obtained after step commands in *A* (*open circles*) and current obtained after the ramp depolarization (note that there is a good agreement between both methods). *C*, *I–V* plots from ramp responses were transformed to permeabilities by the Goldman-Hodgkin-Katz constant field equation for current. Note that the permeability function is reasonably well fitted by a Boltzmann function. *D*, Comparison of the normalized activation plots from ramp and tail currents (measured at the *arrow* in *A*). The *solid line* is the Boltzmann fit derived from the ramp data in *C*.

1 ($\gamma(V_m)$) was not near zero (~20–30 mV below the apparent reversal potential of +55 mV), the permeability estimates could usually be fitted reasonably well with a Boltzmann function of the form

$$P(V_m) = \frac{\alpha}{1 + \exp(-(V_m - V_h)/V_c)}, \quad (2)$$

where V_h = half-activation voltage, V_c = slope factor, and α = maximum permeability. An example of such a fit is shown in Figure 1*C*. Activation plots generated in this way usually agreed reasonably well with activation plots generated from tail current amplitudes (Kay and Wong, 1987). Tail currents produced by traditional step protocols (Fig. 1*A*) were used to estimate whole-cell conductance using the equation

$$G(V_{step}) = I_{tail}/(V_{tail} - V_{rev}), \quad (3)$$

where V_{step} = membrane potential during the step preceding the tail, I_{tail} = tail current immediately after the tail-eliciting step, V_{tail} = the voltage during the tail, and V_{rev} = reversal potential of the current. Although only an approximate value of V_{rev} was available, this calculation yields an estimate that is within a multiplicative constant of the true value. By normalizing amplitudes, estimates of conductance can be compared to those derived from the current–voltage relationship and ramps. As shown in Figure 1*D*, the Boltzmann fit derived from the ramp currents provides an excellent fit of the tail current data (measured 150 μsec into the tail), suggesting that each of the three independent approaches (peak currents, ramps, and tail currents) yield similar estimates of the voltage dependence of Ca^{2+} channel gating. It should not be inferred, however, that this cell (or others with similar properties) express a single species of Ca^{2+} channel. In fact, we will present evidence that this is not the case (see below). The fits were used only for descriptive purposes; they have the advantage of being able to summarize activation data succinctly with three parameters: α, V_h, and V_c.

Retrograde labeling. Injections of fluorescent rhodamine-impregnated microbeads into the substantia nigra were made 2–12 d prior to the experiment. Animals were anesthetized with a mixture of ketamine (100 mg/kg) and xylazine (100 mg/kg) intraperitoneally. A suspension of microbeads in saline (Lumafluor, Inc., Ravada, CO) was injected via a stereotaxically placed microsyringe needle. Three injections of 3 μl each were made on each side separated by 0.5 mm in the rostrocaudal direction. Bead injections into the substantia nigra typically labeled about half the cells in frontal sections of the striatum as well as about half of the cells acutely dissociated from this region. Neurons from these animals were dissociated as described above. Retrogradely labeled neurons were identified under epifluorescent illumination (Surmeier et al., 1992). An example of a retrogradely labeled neostriatal neuron viewed with normal illumination (bottom) and epifluorescence (top) is shown in Figure 2.

Expression profiling. Neostriatal neurons were dissociated, identified and recorded from as above except that the patch-clamp electrode was backfilled with a solution containing dNTPs, oligodT-T7 primer, and reverse transcriptase; positive pressure was maintained on the electrode during the approach to avoid entry of cellular debris. After seal rupture, the electrode and attached cell were lifted into a stream of control salt solution and the cell was sucked into the pipette. First-strand cDNA

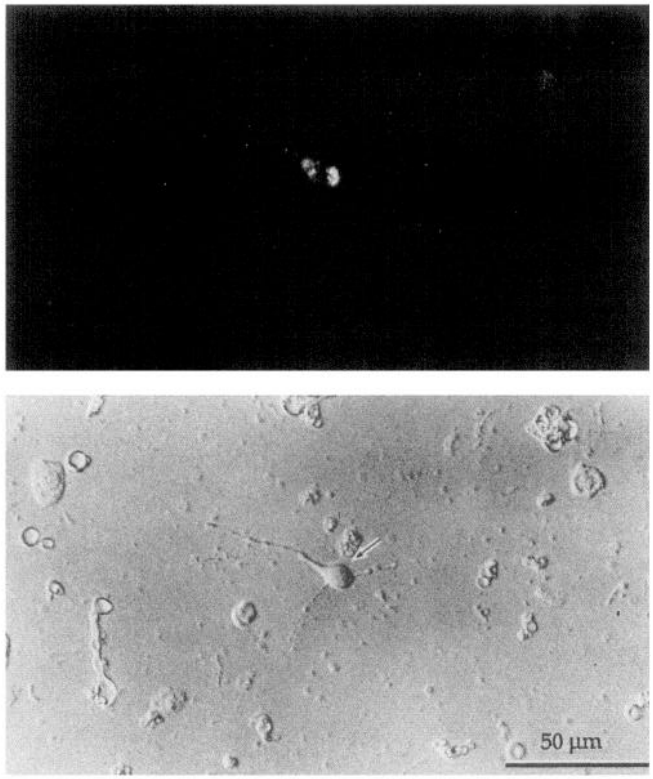

Figure 2. Retrogradely labeled striatonigral neuron. *Bottom,* Photomicrograph of an acutely isolated neostriatal neuron viewed with normal illumination. *Top,* The same field when viewed with epifluorescent illumination with a rhodamine filter set. The neuron was dissociated from a P29 rat 2 d after rhodamine bead injection in the substantia nigra.

synthesis and amplification proceeded as previously described (Van Gelder et al., 1991; Eberwine et al., 1992). An antisense RNA (aRNA) probe was made by incorporating radiolabeled nucleotides into the second round of aRNA amplification as described in Eberwine et al. (1992). BamHI-digested cDNAs for rbA, rbB, and rbC Ca^{2+} channels (Snutch et al., 1991), plasmid Bluescript vector (pBS) and other marker cDNAs were denatured and then 1 μg of each was loaded in 10× SSC onto nitrocellulose membranes using a Schleicher and Schuell slot blotter. The nitrocellulose was baked for 4 hr at 80°C in a vacuum followed by prehybridization for 5 hr at 50°C with 50% formamide, 6× SSC, 1× Denhardt's, and 50 μg/ml salmon sperm DNA. The radiolabeled aRNA from each cell was added to a filter and hybridized at 50°C for 48 hr. After hybridization, the filters were washed once for 30 min in 2× SSC, 1% SDS followed by two 30 min washes in 0.1× SSC, 1% SDS at 50°C. After washing, the filters were apposed to XAR film for 48 hr at −80°C with an intensifying screen. Autoradiograms were digitally scanned into a Macintosh computer, processed with Adobe PHOTOSHOP (ver. 2.5, Adobe Systems, Mountain View, CA) and printed on a Tektronix Phaser printer (Tektronix, Beaverton, OR).

Results

Activation properties

From negative holding potentials (< −80 mV), short depolarizing voltage steps evoked inward current. The rate of activation increased with progressively stronger depolarizations. Little inactivation was evident within the time frame of these short steps (10–30 msec). An example of the currents evoked by a series of depolarizing steps is shown in Figure 3*A*. A plot of the peak current as a function of membrane potential is shown in Figure 3*B*. Typically, currents activated near −40 mV and peaked near 0 mV. Using the GHK constant current equation (Eq. 1), the

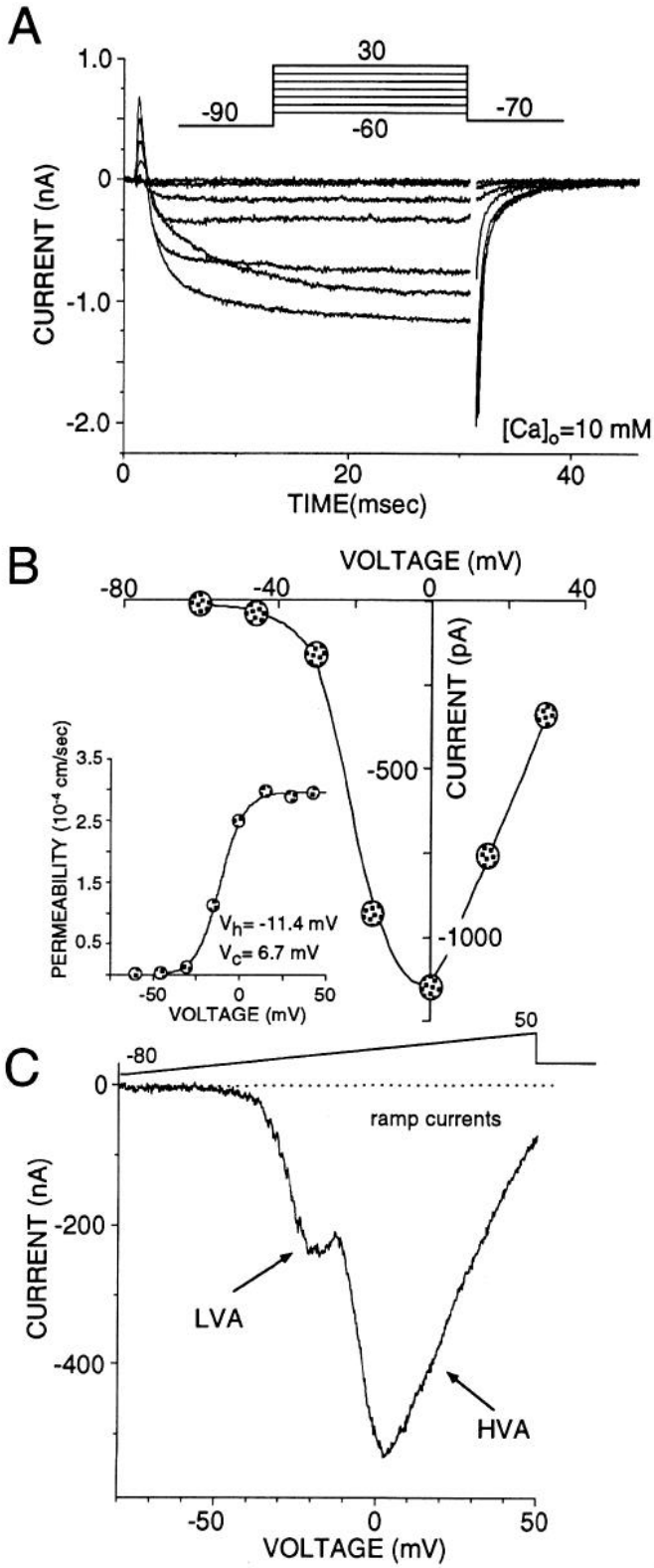

Figure 3. Neostriatal Ca^{2+} currents are largely of the HVA type. *A,* Currents elicited in 10 mM Ca^{2+}, *inset* at *top* illustrates the stimulation protocol. *B, I–V* plot constructed with peak currents in *A* (*dotted circles*); the *solid line* is a spline fit of the data. *Inset* illustrates the activation plot obtained by applying the constant field transformation to the *I–V* plot data. Note that maximal permeability corresponds to the linear portion of the *I–V* plot. Even if the tails have a slow component (*A, C*; see text) a low-threshold "hump" was not detected in the *I–V* plot. *C,* In a small percentage of neurons (< 10%, $n = 256$), a distinct "shoulder" or secondary peak was detected in the *I–V* plot.

current–voltage relationship could be converted into an estimate of permeability and fitted with a Boltzmann function (see Fig. 1); these estimates could then be used to compare the voltage dependence of calcium currents in different cells. The inset in Figure 3*B* shows the conversion for the data plotted above. In this cell, the half-activation voltage was −11.4 mV and the slope factor was 6.7 mV. The average half-activation voltage (V_h) in a subset of our sample in which 2 mM Ca^{2+} or 5 mM Ba^{2+} was used as the charge carrier was −5.7 ± 8.8 mV (±SD, n = 23), and the average slope factor (V_c) was 6.22 ± 0.72 mV (±SD).

As judged from the responses to voltage steps (10–300 msec) and ramps, the vast majority of adult (>4 weeks postnatal) neostriatal neurons (~90%, n = 256) did not exhibit a significant low-voltage-activated current (LVA or T) component. This was unexpected, as LVA currents are present in cultured embryonic striatal neurons (Bargas et al., 1991) and in acutely isolated or cultured neurons from early postnatal animals (<P7, n = 23). Our inability to see these currents was not a consequence of our recording conditions as we were able to see them on occasion in adult neurons. An example of ramp currents taken from one such cell is shown in Figure 3*C*. There was no discernible correlation between the presence of LVA currents and neurite length, somatic diameter, or shape. LVA currents were not seen in any of the retrogradely labeled striatonigral neurons studied (n = 18) or in cells subjected to single-cell aRNA amplification that were of a projection phenotype (n = 5). It is our working hypothesis that these currents are expressed only in interneuronal or juvenile phenotypes and not in adult medium spiny projection neurons.

Effects of changes in charge carrier

In situ, the concentration of extracellular Ca^{2+} ($[Ca^{2+}]_o$) is thought to be closer to 2 mM than 5 or 10 mM. Because most neostriatal neurons are relatively small (<15 μm diameter), we normally used higher concentrations of charge carrier to increase the resolvability of currents. However, alterations in divalent cation concentration introduce changes in current kinetics (Hille, 1992). These changes vary to some extent among cell types. To determine how Ca^{2+} currents were affected in neostriatal neurons, ramp currents were recorded in 2, 5, and 10 mM $[Ca^{2+}]_o$. An example of currents recorded under these different conditions is shown in Figure 4*A*. As predicted by the GHK current equation, peak current amplitude increased with increasing divalent concentration. Plots of the peak current as a function of Ca^{2+} concentration were approximately linear in the range tested, as previously reported (Hagiwara and Ohmori, 1982).

In addition to altering peak amplitude, elevating $[Ca^{2+}]_o$ appeared to shift the voltage dependence of the current gating toward depolarized potentials. Permeability estimates calculated using the GHK equation confirmed this inference (Fig. 4*B*); shown in the inset are the changes in the "driving force" term in the GHK equation [$\gamma(V_m)$ in Eq. 1] for 2, 5, and 10 mM Ca^{2+}. The half-activation voltage shifted approximately 10 mV for each twofold increase in concentration (V_h = −10.1, 0.2, 10.3 mV) whereas the slope factor increased only slightly (V_c = 5.4, 6.3, 7.3 mV). Similar shifts were seen in three other neurons.

Ca^{2+} channels typically allow other divalent ions, such as Ba^{2+}, to pass readily through them. Because it does not substitute well for Ca^{2+} in activating intracellular enzymes associated with the "rundown" or inactivation of currents, Ba^{2+} was used in most experiments rather than Ca^{2+}. The permeation and charge screening effects of Ba^{2+} and Ca^{2+} on HVA currents are not identical, however. As we are interested in how Ca^{2+} currents participate in normal behavior of neostriatal neurons, we examined the effects of Ba^{2+} substitution on the properties of Ca^{2+} currents in our cells. The substitution of 10 mM $[Ba^{2+}]_o$ for 10 mM $[Ca^{2+}]_o$ nearly doubled peak current amplitude and shifted its position toward more negative potentials (Fig. 4*C,D*). Similar changes in HVA currents with Ba^{2+} substitution have been reported in other neurons (e.g., Wilson et al., 1983; Hernandez-Cruz and Pape, 1990). The shift in voltage dependence of the whole-cell currents with Ba^{2+} substitution can be seen more clearly in the permeability estimates shown in Figure 4*D*. The half-activation voltage shifted −8.8 mV (from 5.5 mV to −3.2 mV), and the slope factor decreased 1.75 mV (from 8.25 mV to 6.5 mV). Similar shifts were seen in three other cells (ΔV_h, μ = 8.1 ± 3.2 mV; ΔV_c, μ = 1.43 ± 0.6 mV). The ratio of maximum permeabilities (P_{Ba}/P_{Ca} = 1.32) in this neuron was similar to those seen in other cells (1.24, 1.45, 1.34).

Alterations in the concentration of extracellular Ba^{2+} had a qualitatively similar effects as those seen following changes in $[Ca^{2+}]_o$. Increasing $[Ba^{2+}]_o$ from 5 to 10 mM increased current amplitudes and shifted the peak of the current–voltage relationship toward more depolarized potentials (Fig. 4*E*). In contrast to the experiments with Ca^{2+}, doubling the Ba^{2+} concentration did not produce a significant change in the current amplitudes near threshold (compare Fig. 4*A,E*). Calculation of the permeability estimates for this neuron are shown in Figure 4*F*. The half-activation voltage was shifted 7.0 mV (from −10.2 to −3.2 mV) by increasing the $[Ba^{2+}]_o$ from 5 to 10 mM; the slope factor was increased 0.7 mV (from 5.8 to 6.5 mV). Similar results were obtained in two other neurons (ΔV_h = 5.6, 6.4 mV; ΔV_c = 0.5, 0.8 mV). The inset shows the Boltzmann fits at these two concentrations of Ba^{2+} on a normalized scale. Also shown for comparison is the Boltzmann fit of the estimates in 10 mM Ca^{2+}. Although the voltage dependence of gating (as judged by the permeability fits) was considerably different in 5 mM $[Ba^{2+}]_o$ and 10 mM $[Ca^{2+}]_o$, the voltage dependence in 2 mM $[Ca^{2+}]_o$ (approximately physiological concentration) and 5 mM $[Ba^{2+}]_o$ was very similar in most cells (compare Figs. 3*B*, 4*F*). Because of this similarity and the fact that Ba^{2+} increased current amplitudes at most potentials, it was used as the charge carrier in many of our subsequent experiments.

Inactivation properties

Holding the membrane at potentials more depolarized than around −80 mV led to a reduction in the amplitude of evoked currents. The voltage dependence of this process was first studied by examining the effects of 3 sec conditioning steps on the currents evoked by a test step to 0 mV. As the conditioning steps became progressively more depolarized, the current evoked by the test step became smaller (Fig. 5*A*). Plots of the peak current during the test step as a function of conditioning voltage were monotonically decreasing (Fig. 5*B*). These data were fitted with a Boltzmann functions of the form

$$I/I_{max} = \frac{1}{1 + \exp\left(\frac{V_{pp} - V_{h1}}{V_{c1}}\right)} \quad (4)$$

where V_{pp} = voltage of the prepulse, V_h = half-activation voltage, and V_c = slope factor. In a subset of cells (n = 14), the half-inactivation voltage was −26.6 ± 7.0 mV (±SD; range, −36

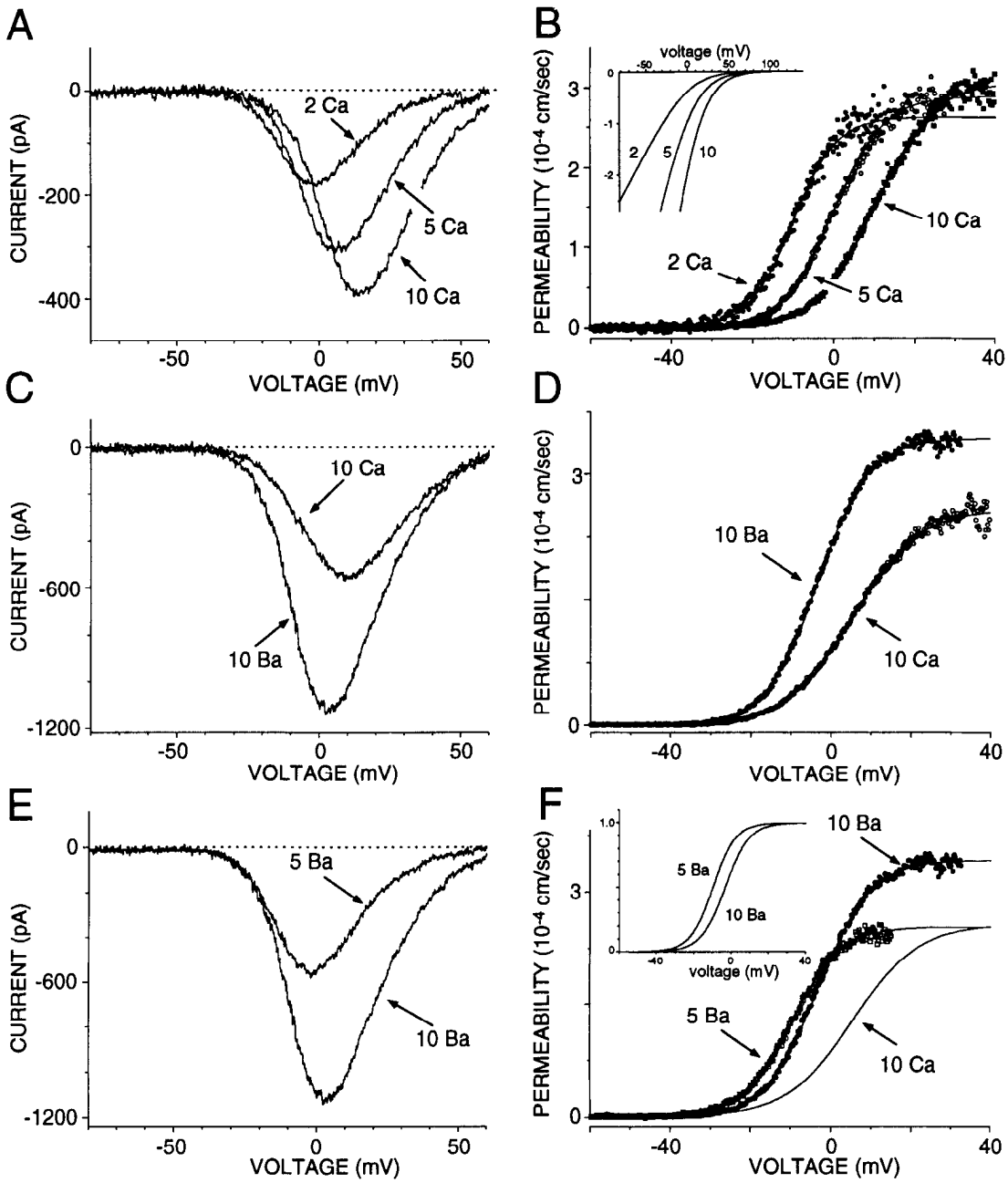

Figure 4. The effects of ionic substitution on current–voltage relationships. *A*, *I–V* plot behavior after increasing extracellular Ca^{2+} concentration. *B*, Corresponding activation plots after constant field transformation of the *I–V* plots in *A*. *Inset*, Constant field rectification after increasing extracellular Ca^{2+} concentration. *C*, Effects of Ba^{2+} substitution. *D*, Corresponding activation plots for *C*. *E*, Effects of increasing Ba^{2+} concentrations. *F*, Corresponding activation plots for *E*. *Inset*, Normalized activation; a fit of activation at 10 mM Ca^{2+} is included.

to −15 mV). Similar values have been reported for HVA currents in a number of other cell types (Kostyuk et al., 1981; Fox et al., 1987a; Tsien et al., 1988; Jones and Marks, 1989b; Mendelowitz and Kunze, 1992; Mynlieff and Beam, 1992). However, in over half of the cells studied (8 of 14), there was a clear inflection in the plot of peak current as a function of conditioning voltage. These data sets were only well fitted with a sum of Boltzmann functions, as shown in Figure 5*B*.

Two mechanisms are thought to mediate inactivation in paradigms such as this one. One is voltage-dependent inactivation, as seen in a wide variety of other channel types; the other mechanism is Ca^{2+} dependent (Brehm et al., 1980; Chad et al., 1984; Schroeder et al., 1990). To help distinguish between these processes, the peak current–voltage relationship during the condition step was plotted on the same scale as the inactivation data (Fig. 4*B*, open symbols); plots of total charge entry (integral of the current waveform) were similar but peaked at more negative potentials. In this cell, peak current was reduced 20% before there was any detectable current entry during the conditioning step. This proportion was similar to that seen in other cells ($\mu = 24 \pm 13\%$, $n = 10$). Although the second, larger component of inactivation began as Ca^{2+} began to enter during the conditioning steps, the inactivation was not strictly dependent upon the magnitude of Ca^{2+} entry as inactivation became progres-

sively larger above 0 mV, yet the inward currents declined at these potentials. This pattern was very similar when Ba^{2+} was the charge carrier instead of Ca^{2+}—arguing that a substantial component of both phases of inactivation was voltage dependent, rather than Ca^{2+} dependent.

An examination of the tail currents evoked by the test step following conditioning prepulses also suggested that more than one current was present. With negative holding potentials and short test steps (10–30 msec), tail currents at −70 mV had two clear exponential components: one with a time constant near 400 μsec and another, slower one with a time constant of a few milliseconds. Progressively more depolarized conditioning prepulses had no effect on the time constant of the slower component (although its amplitude was reduced), but the time constant of the faster component became significantly shorter (Fig. 5*C*). The change in the shorter time constant was close to what would be expected if a slowly deactivating N-type current were being inactivated, revealing a current that was more resistant to inactivation, such as an L-type current (see Figs. 8, 10; Kostyuk and Shirikov, 1989; Regan, 1991; Regan et al., 1991).

It was evident in these experiments that the inactivation process had not reached steady state at the end of the 3 sec conditioning steps. Inactivation with either Ca^{2+} or Ba^{2+} as the charge carrier took considerably longer to stabilize. Short conditioning steps (e.g., 300 msec) to potentials above 0 mV typically produced less than a 20% reduction in the peak current evoked by the test step (0 mV). In some cells, virtually no inactivation was produced by these short conditioning steps. To gain a clearer picture of the kinetics of inactivation and its impact on the current–voltage relationship, ramp currents were examined as a function of time after changing the holding potential from −90 mV to near the current threshold at −40 mV (Fig. 6). Ba^{2+} (5 mM) was used as the charge carrier to minimize the effects of current entry during the test pulse on the development of changes in the current. Holding at potentials above the threshold for evoking detectable current (−30 to −35 mV) led to the progressive elimination of all currents. Recovery from this inactivation was typically not achievable within the time frame of most recordings (20–30 min).

As shown in Figure 6*A*, holding the membrane at −40 mV for several minutes produced a substantially larger reduction in current amplitude than the 3 sec conditioning prepulses to −40 mV. The development was exponential in time course with a time constant of approximately 53 sec; similar results were obtained in other cells ($\mu = 42 \pm 18$ sec, $n = 6$). Subtraction of the currents evoked at −90 mV from those evoked after stabilization of the currents at −40 mV was used to determine the voltage dependence of the inactivating current (Fig. 6*B*). The threshold and peak of the inactivating current were more depolarized than the current remaining after the change in holding potential. The permeability estimates for the inactivating and noninactivating currents were reasonably well fitted between −40 and +20 mV with single Boltzmann functions. The inactivating current had a more depolarized half-activation voltage ($\mu = -7.3 \pm 5.3$ mV, $n = 6$) than did the noninactivating current ($\mu = -15.2 \pm 6$ mV, $n = 6$).

The inactivating and noninactivating currents also differed in activation kinetics when tested with step depolarizations (Fig. 6*D*). As above, subtraction was used to isolate the inactivating part of the current. In the first few hundred microseconds, the kinetics of the evoked current were independent of holding potential. Thereafter, however, currents diverged in waveform.

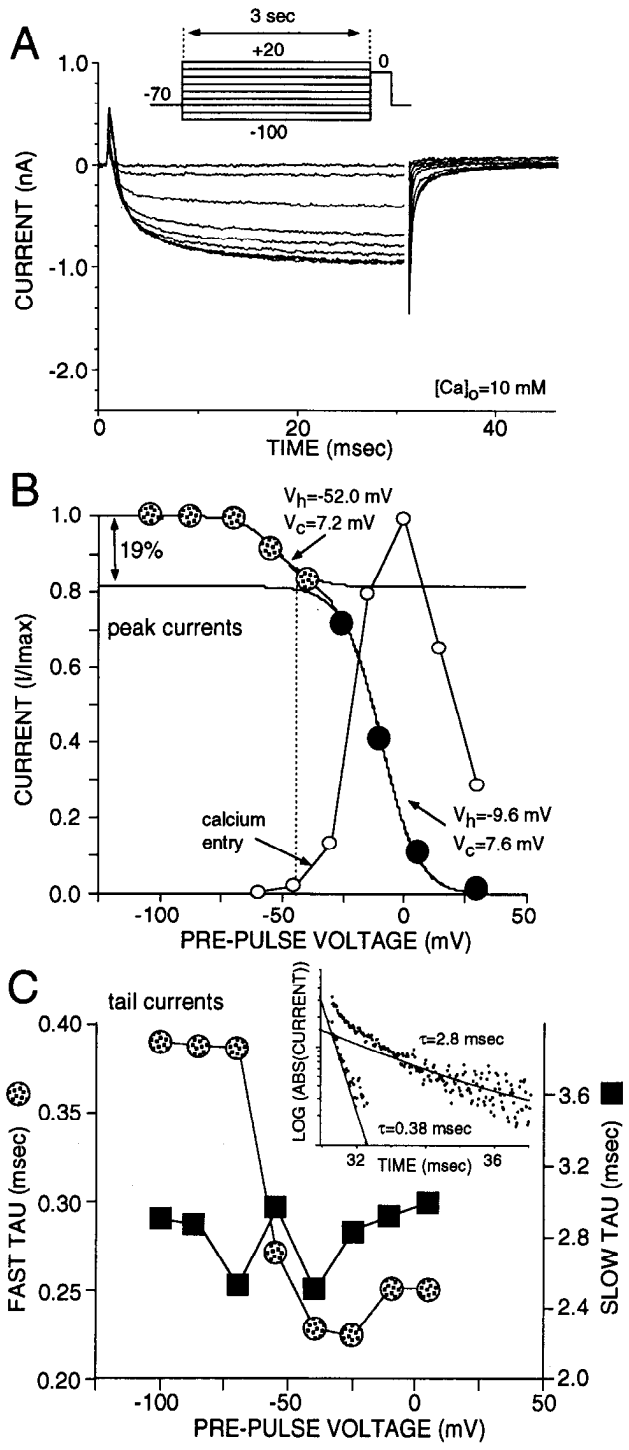

Figure 5. Ca^{2+} currents display voltage-dependent inactivation. *A*, Ca^{2+} currents elicited by 0 mV commands after previous depolarizations of 3 sec (stimulation protocol at *inset* on *top*; prepulses evoked currents not shown). Note a virtually complete inactivation. *B*, Two Boltzmann functions were needed to fit the inactivation plot using maximal current amplitudes from *A* (*dotted* and *solid circles*), indicating that two different processes were involved. An inverted and normalized *I–V* plot from the same cell was superimposed (*open circles*) to indicated that there was little or no Ca^{2+} entry during the first component of inactivation. *C*, Deactivation currents from *A* exhibit two components: fast and slow (*inset*). The fast component became faster with more depolarizing prepulses (*dotted circles*). The slower component did not change kinetics with increasing depolarizations. The currents unblocked by Cd^{2+} were subtracted from all records.

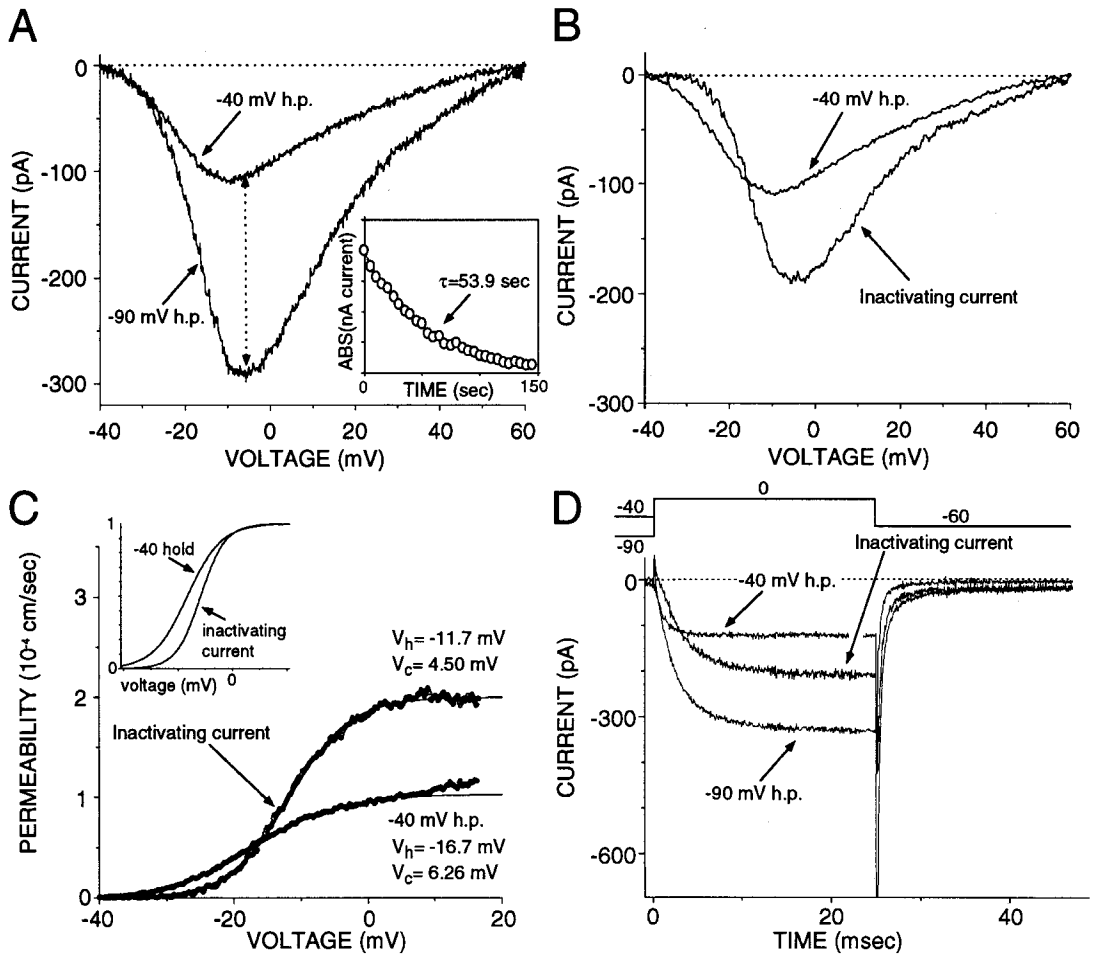

Figure 6. A change in holding potential produces a change in the voltage dependence of the whole-cell current. *A*, Responses to ramp depolarizations from two different holding potentials are compared. Note a displacement of peak current along the voltage axis (*double-headed arrow*). *Inset*, Development of inactivation needs tens of seconds to be complete. *B*, Identification of the inactivating current by subtraction the current evoked from −40 mV from the current evoked from −90 mV. *C*, The current evoked from −40 mV had a more negative half-activation voltage; the inactivating current has a more positive half-activation voltage. *D*, Comparison of the responses to step depolarizations at the two holding potentials revealed that the inactivating current (obtained by subtraction) appeared to activate more slowly than the "noninactivating" current.

From a holding potential of −40 mV, the currents evoked by the test step plateaued rapidly whereas those evoked from −90 mV did not reach their maximum until near the end of the pulse. The difference currents (computed by subtracting the currents evoked from −40 mV from those evoked from −90 mV) were slow in onset and did not plateau until late in the step. One obvious difficulty in the interpretation of the subtracted records is that holding at depolarized potentials may significantly alter the distribution of channels in closed states leading to the open state (e.g., Harrington and Lingle, 1992; however, for a discussion see Jones and Marks, 1989a). In so doing, the kinetics of activation (transition to the open state) would appear faster from depolarized potentials without changing the channel types contributing to the evoked current. Although this certainly true of Ca^{2+} channels in our cells (data not shown), it is unlikely to entirely explain the difference in kinetics at the two potentials. As shown below, slower onset kinetics were also seen in the ω-CgTx–sensitive portion of the current that was lost at depolarized holding potentials.

Pharmacological Properties

Cd^{2+} sensitivity. All of the voltage-sensitive currents observed in our recording conditions were blocked by micromolar concentrations of cadmium ions (Cd^{2+}) (200–400 μM). Although large differences in the affinity of HVA currents for Cd^{2+} have not been reported, a quantitative description of the block was obtained to determine whether current types could be separated on this basis. As shown in Figure 7*A*, Cd^{2+} was a potent blocker of currents evoked with a voltage ramp from negative holding potentials (−90 mV). A plot of the peak current amplitude as a function of Cd^{2+} concentration could be fitted with a single isotherm of the form

$$I = \frac{I_{max}}{1 + \left(\frac{[Cd^{2+}]}{IC_{50}}\right)^n}, \quad (5)$$

where $n = 1$. Hill plots (inset) consistently were best fitted by lines with slopes less than 1, suggesting that multiple binding sites (or cooperativity) were present (Swandulla and Armstrong, 1989). In three neurons, the mean IC_{50} was 1.3 μM, which is very close to that reported for HVA currents (Narahashi et al., 1987; Kasai and Neher, 1992). Changing the exponent of the fitted isotherm to 0.7 produced only a modest change in the IC_{50} (~10%). Note that current across the entire voltage range was decreased by Cd^{2+} without revealing a relatively resistant

portion (Fig. 7*A*). In contrast, immature neurons did not behave in this way. Shown in the inset of Figure 7*A* are ramp currents recorded in 10 mM Ba^{2+} from a P4 neuron cultured for 48 hr. Cd^{2+} (200 μM) effectively blocked all but a small component of the lowest-threshold part of the evoked current. With washing, the LVA component recovered rapidly ("early wash") whereas the HVA components recovered more slowly ("late wash"); this kinetic pattern is consistent with the affinity differences these currents display for Cd^{2+}. Similar results were observed in most (14 of 15) neurons cultured from embryonic (E18) or P4 rats. These findings reinforced the view that in adult medium-sized neurons virtually all current was due to HVA-type channels (Fox et al., 1987; Narahashi et al., 1987; Kaneda and Akaike, 1989).

Dihydropyridine sensitivity. A more profitable approach to fractionating the whole-cell calcium currents employed organic channel blockers. To determine whether L-type channels contributed to the whole-cell currents, their sensitivity to the dihydropyridine antagonist nifedipine was examined. As shown in Figure 8*A*, nifedipine at saturating concentrations (5–10 μM) reversibly blocked a significant fraction of the current evoked by a step to 0 mV from negative holding potentials. Although the percentage block was greater at depolarized holding potentials, the absolute magnitude of the nifedipine block was only modestly sensitive to holding potential between −40 mV and −90 mV (Fig. 8*B*; the inset bar shows the amplitude of the block in Fig. 8*A*). The median percentage block at a holding potential of −90 mV was 21% (n = 13) and 43% at a holding potential of −40 mV (n = 11). The was no significant difference in the absolute magnitudes of the block at these two holding potentials. Nor was there any dramatic shift in IC_{50} values at the two potentials; the median IC_{50} was 0.5 nM at −40 mV (n = 9) and 0.8 nM at −90 mV (n = 8) (data not shown).

In addition to their pharmacological differences, L-type channels in other neuronal types appear to deactivate more rapidly than other HVA currents (Kostyuk and Shirokov, 1989; Regan et al., 1991). To test whether this was also true in neostriatal neurons, the deactivation tails of the nifedipine-sensitive component of the current were fit with a sum of exponentials. In all cases (n = 5), tail currents were well fitted with a single exponential (Fig. 8*C,D*); the median time constant at −80 mV was 183 μsec, which is very close to that reported by Regan et al. (1991).

In the presence of the mixed dihydropyridine agonist (±)Bay K 8644, the deactivation kinetics of L-type currents are slowed (Brown et al., 1984; Fox et al., 1987b). Figure 9*A–C* shows that a similar modulation can be seen in neostriatal neurons. Bay K 8644 (2 μM) reversibly enhanced the magnitude of the current evoked by depolarizing steps (Fig. 9*A*) and significantly slowed the rate at which the whole-cell current decayed upon repolarizing to −55 mV (Fig. 9*B*). Bay K 8644 also increased peak current and produced a leftward shift in the current–voltage relationship (Fig. 9*D*), as seen in a number of other cell types (Sanguinetti et al., 1986; Kass, 1987).

ω-Conotoxin GVIA sensitivity. In many mammalian neurons, a large component of HVA current is blocked by the marine snail *Conus geographus* toxin ω-conotoxin GVIA (ω-CgTx) (Fox et al., 1987a; McCleskey et al., 1987; Artalejo et al., 1992). We operationally defined N-type current as this ω-CgTx–sensitive current. From a holding potential of −90 mV (Fig. 10*A*), ω-CgTx blocked about a quarter of the peak current (this percentage varied, see below). Holding at −40 mV, however, apparently

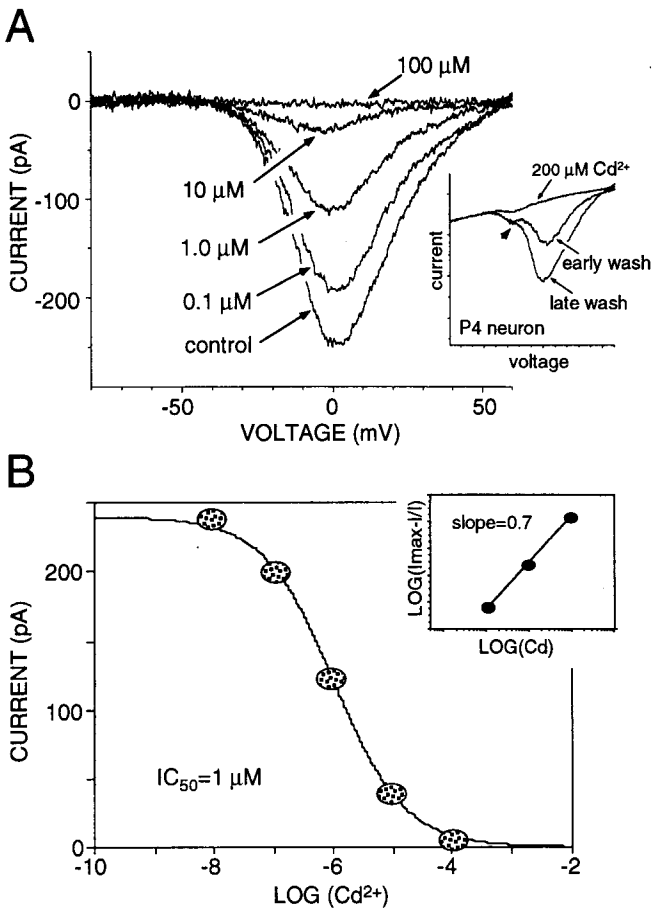

Figure 7. Cadmium blocks the whole-cell current with an IC_{50} near 1 μM. *A*, Effects of increasing Cd^{2+} concentrations on currents evoked by ramp depolarizations (5 mM Ca^{2+}). *Inset* shows a current–voltage plot from a P4 neostriatal neuron maintained in culture for 48 hr before recording. The traces show that 200 μM Cd^{2+} incompletely blocks the LVA current and the block of this component reverses quickly (*early wash*). Note the difference in pattern with the adult neuron. *B*, Dose–response relationship. *Inset*, Hill plot of the dose–response data. The line fitting these points had a slope of 0.7.

inactivated the component of the current sensitive to ω-CgTx (Fig. 10*B*). This is consistent with the well-described sensitivity of N-type channels to holding potential (Fox et al., 1987a; Aosaki and Kasai, 1989; Takahashi et al., 1989).

N-type currents have been reported to deactivate more slowly than L-type currents (Kostyuk and Shirokov, 1989; Regan et al., 1991). This also appears to be the case in neostriatal neurons. The ω-CgTx–sensitive tail current obtained by subtraction could be well fitted with a single exponential (Fig. 10*C,D*); the mean deactivation time constant at −80 mV was 302 ± 46 μsec (n = 5).

Another commonly reported characteristic of the block by ω-CgTx is its irreversibility. This was not always the case in our experiments. In a significant fraction of neurons, the block produced by ω-CgTx (1–4 μM) partially reversed within minutes of beginning superfusion with control solution. The distribution of reversal percentages (measured 2 min after returning to control solution) in a sample of 40 neurons is shown in Figure 11*A*. Because it has been reported (Aosaki and Kasai, 1989; Williams et al., 1992) that a component of the DHP-sensitive current can be transiently blocked by ω-CgTx, we attempted to determine

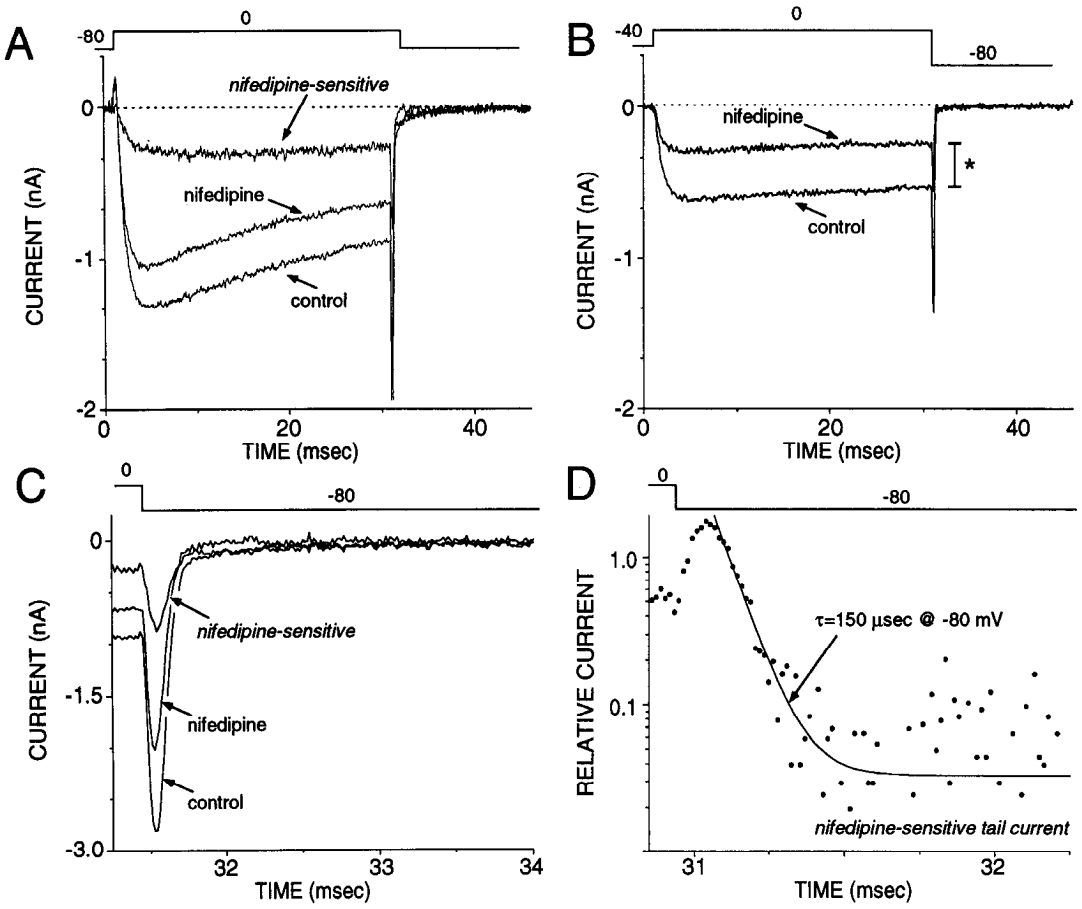

Figure 8. Nifedipine blocks a rapidly activating and deactivating current. *A* and *B*, Currents evoked by step depolarizations to 0 mV from a holding potential of −80 mV (*A*) or −40 mV (*B*) before and after the application of 5 μM nifedipine. The nifedipine-sensitive current was obtained by subtraction. Note that proportion of current blocked increased after holding at −40 mV. *C*, Plot of tail currents evoked in *A*. The nifedipine-sensitive current was determined by subtraction. *D*, Semilogarithmic plot and fit of the nifedipine-sensitive tail current.

whether our transient block could be explained in a similar way. This hypothesis has three obvious implications. First, if the transient block were of L-type channels, then changing the holding potential from −90 mV to −40 mV should not significantly attenuate its magnitude (because L-type currents were not markedly affected by such a change). This was not the case. As shown in Figure 11*B*, the transient component of the block was nearly eliminated (block was 12% of control) by changing the holding potential.

A second prediction of the hypothesis is that the block produced by the coapplication of ω-CgTx and nifedipine should be less that the sum of the blocks produced by each antagonist on its own (subadditivity). As shown below (Fig. 12), this also was not the case. A third prediction is that is that the slow component of the Bay K 8644–enhanced tail currents should be transiently reduced by ω-CgTx. As shown in the inset of Figure 11*B*, the Bay K 8644 enhanced tail current is not reduced by ω-CgTx, although the peak current clearly was reduced, suggesting that the block was of a non-L-type current.

Another possibility was that the toxin we were using had been degraded in some way. To check for this possibility, we isolated neurons from the globus pallidus and applied ω-CgTx (2 μM) (previous work on these neurons had revealed that the ω-CgTx never completely reversed with washing). As shown in Figure 11*C*, the block by ω-CgTx in this pallidal neuron only partially reversed with washing (similar results were obtained in two other cells). Application of the same working ω-CgTx solution to an acutely isolated neostriatal neuron 20 min later (Fig. 11*C*) produced a completely reversible block of whole-cell currents, arguing that the reversibility was not a consequence of toxin degradation (or enzyme treatment).

An examination of the kinetics of the ω-CgTx block and its reversal suggested that the dissociation step alone was different. The time constant of the onset of the block was 7.6 sec and the recovery time constant was 12.6 sec. In three other cells showing reversible block, the time constants of block were similar (τ = 5.8–8 sec), whereas the washoff time constants were generally slower than the example in Figure 11*B* (τ = 13–50 sec). Based upon the kinetics in the example of Figure 11*B*, the on-rate was estimated to be 1×10^4 sec^{-1} M^{-1} (which is comparable to that reported in neuroblastoma cells by Kasai and Neher, 1992), whereas the off-rate (0.079 sec^{-1}) was, of course, much faster than that predicted by an essentially irreversible block. One possible explanation of the enhanced off-rate is that a portion of the binding domain was altered by enzyme treatment. However, shortening the digestion time (from 30 to 10 min) or altering the enzyme (papain instead of pronase) did not noticeably alter the reversibility of the block. In accord with this observation are reports of partial reversals of the ω-CgTx block in nonenzymatically dissociated neurons (Plummer et al., 1989; Suprenant et al., 1990).

The reductions in current amplitudes brought about by the

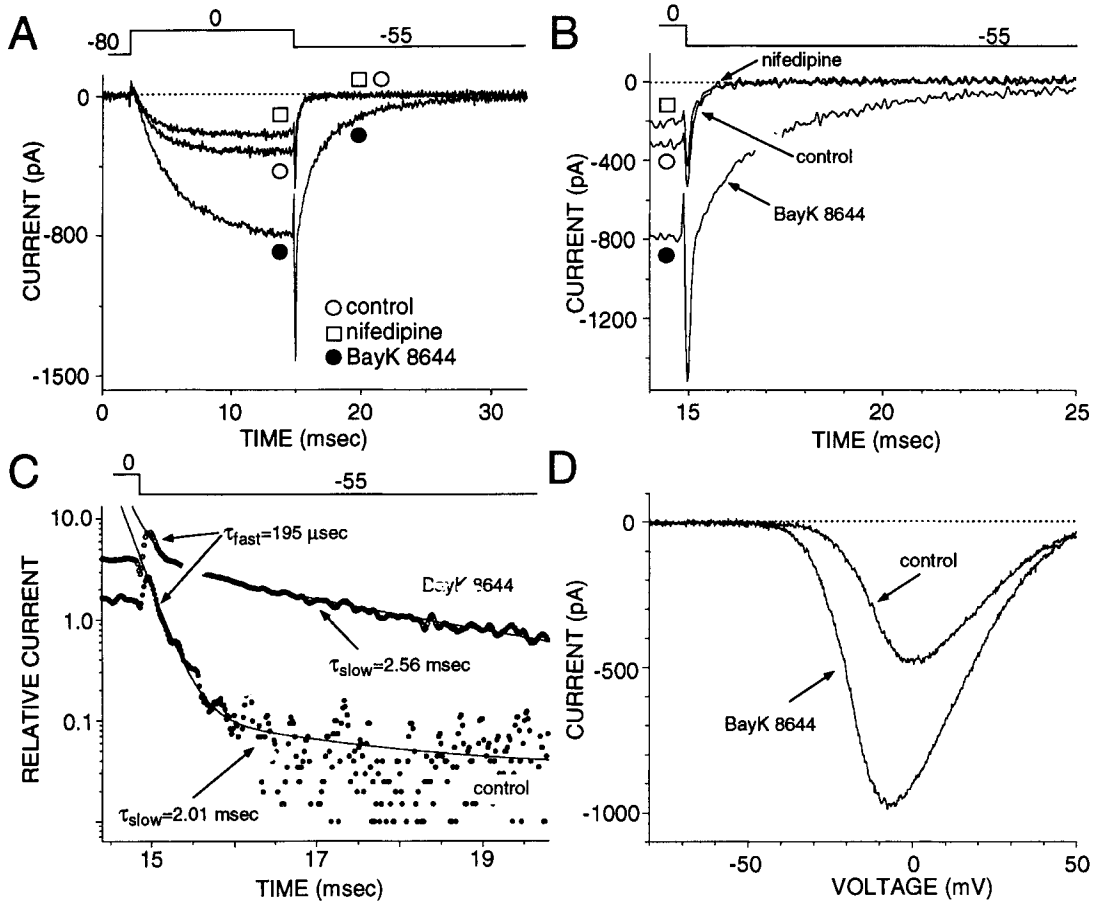

Figure 9. Bay K 8644 enhances whole-cell currents, slows deactivation, and shifts voltage dependence. *A*, Currents before and after nifedipine or Bay K 8644, evoked by step commands to 0 mV from a holding potential of −80 mV. Return potential for tails is −55 mV. Nifedipine was applied first and washed off, and then Bay K 8644 was applied. *B*, A view of tail currents at increased sweep speed. *C*, Fast and slow exponential components can be obtained in control and in Bay K 8644, but the proportion for the slow component increased after Bay K 8644. *D*, *I–V* plots before and after Bay K 8644 constructed from ramp responses. Note an increase in maximal amplitude and a shift to the left of the voltage axis for both peak and threshold.

coapplication of saturating concentrations of ω-CgTx (2–5 μM) and nifedipine (5–10 μM) were largely additive. As shown in the inset of Figure 12*B*, median block produced by ω-CgTx was 25% (n = 17) of the peak ramp current, the median block by nifedipine was 29% (n = 20) and median block by coapplication was 53% (n = 12) of the current. Notice also that a sizable current (median = 44%, n = 12) was resistant to block by either agent. Current records from a cell in which ω-CgTx and nifedipine were sequentially applied are shown in Figure 12. Ramp currents evoked in the absence of blocker, those evoked after the application of ω-CgTx (2 μM), and those after the addition of nifedipine (5 μM, in the presence of ω-CgTx) are shown in Figure 12*A*. After the subtraction of the currents not blocked by Cd^{2+}, the current sweeps were transformed into current–voltage plots shown in Figure 12*B*. Subtraction of the records after ω-CgTx application from the control trace was used to estimate the ω-CgTx–sensitive current (this subtracted record and the control record are shown in Fig. 12*C*). Subtraction of the record after the application of nifedipine from the preceding record was used to obtain the nifedipine-sensitive current (Fig. 12*D*). It was a consistent finding that the nifedipine-sensitive current appeared to turn on and peak at more hyperpolarized potentials than the ω-CgTx–sensitive current (regardless of the order in which the blockers were applied, see below). Also shown in Figure 12*D*, as an inset, is a comparison of the nifedipine-sensitive part of the current and the portion resistant to both blockers.

The permeability estimates derived from the current–voltage plots could be fitted with single Boltzmann functions. Estimates for the ω-CgTx– and nifedipine-sensitive currents are shown in Figure 12*E*; a normalized comparison of these plots is shown in Figure 12*F*.

ω-Agatoxin IVA sensitivity. One plausible hypothesis is that the "resistant" current is carried by a P-type channel (Llinas et al., 1989). A specific blocker of this current is the funnel-web spider toxin ω-agatoxin IVA (ω-AgTx) (Regan et al., 1991; Mintz et al., 1992). The application of saturating concentrations of synthetic ω-AgTx (100 nM; Mintz et al., 1992) consistently reduced peak Ba^{2+} currents. To determine the extent to which an ω-AgTx–sensitive current could account for the residual current seen in the previous experiments, currents were examined after the sequential addition of ω-AgTx (100 nM), ω-CgTx (2–4 μM), and nifedipine (5 μM). A plot of peak current as a function of time after antagonist application is shown in Figure 13*A*. In most cells, the block by ω-AgTx reversed with voltage ramps to +60 mV (Mintz et al., 1992). Representative current traces from this cell are shown in Figure 13*B*. The application of ω-AgTx blocked about 20% of the peak current, with the clearest re-

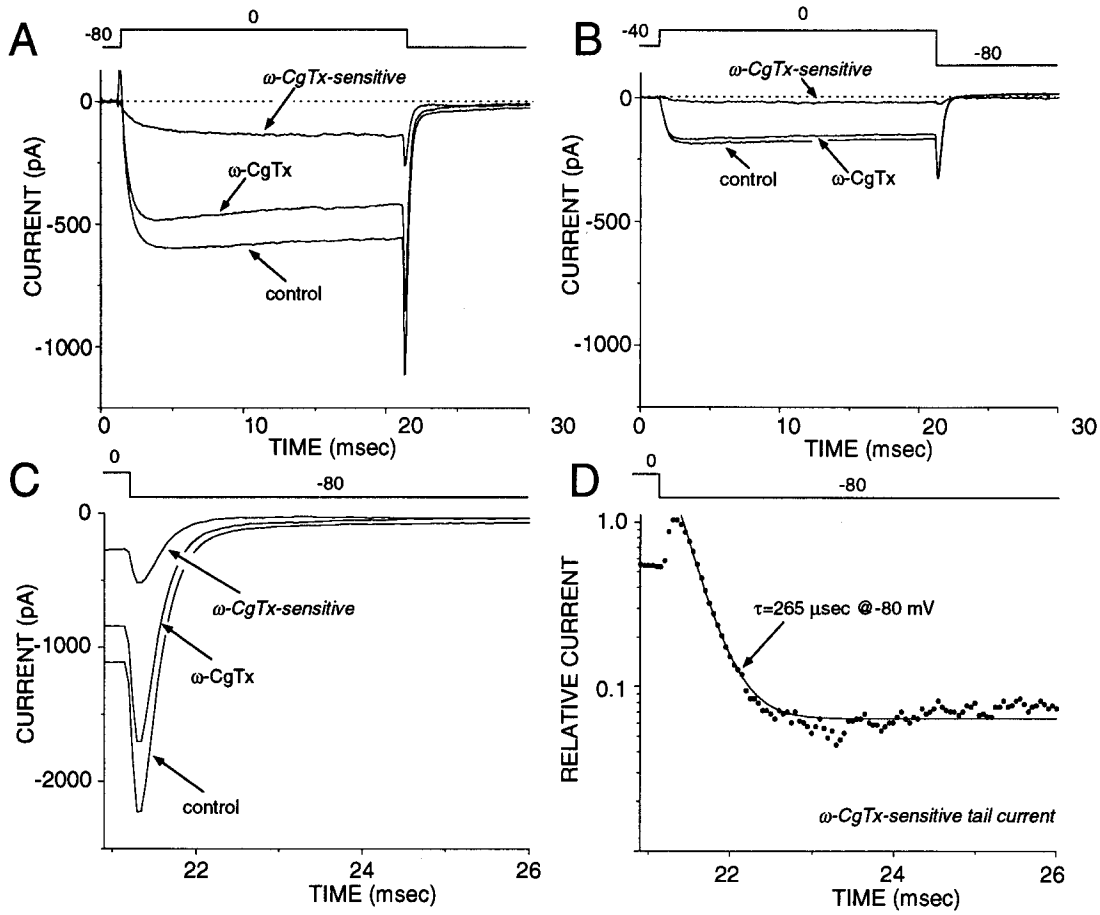

Figure 10. ω-Conotoxin blocks a component of the current that is sensitive to holding potential and deactivates slowly. *A* and *B*, Currents evoked by step depolarizations to 0 mV from a holding potential of −80 mV (*A*) or −40 mV (*B*) before (*control*) and after application of 1 μM ω-CgTx GVIA. ω-CgTx–sensitive current was obtained by subtraction. Note that the proportion of blocked current decreases after depolarizing holding potentials. *C*, Plot of tail currents evoked in *A*. The ω-CgTx–sensitive current was determined by subtraction. *D*, Semilogarithmic plot and fit of the ω-CgTx–sensitive tail current.

ductions being evident with stronger, rather than weaker, depolarizations. The addition of ω-CgTx to the bathing solution resulted in an additional block of about 16% of the peak current. The subsequent addition of nifedipine produced a further reduction in the peak current of about 17% in this cell; in contrast to the reductions produced by the peptide toxins, the nifedipine-induced reductions were most evident at relatively hyperpolarized potentials. In a sample of 19 cells, the median block by ω-AgTx was 19% of the peak current, the median block by ω-CgTx (subsequent to ω-AgTx application) was 15%, and the median block by nifedipine was 27% (after the application of ω-AgTx and ω-CgTx). The median percentage of peak current unblocked by any of these ligands was 38% (the mean was 34 ± 17%). Increasing the concentration of ω-AgTx from 100 nM to 500 nM did not increase the magnitude of its block ($n = 6$), nor was the block by nifedipine increased by using 10 μM instead of 5 μM ($n = 3$).

Although the percentage block by ω-AgTx and nifedipine was relatively consistent in these experiments, there was more variation in the percentage of the peak current blocked by ω-CgTx; the data are summarized in the box plot inset in Figure 13*A*. These data suggest that while ω-AgTx does not affect the dihydropyridine-sensitive current (ω-AgTx did not block Bay K 8644–enhanced tail currents), it may affect a portion of the ω-CgTx–sensitive current, as the median block by ω-CgTx fell from 25% to 16% (following the application of ω-AgTx).

To determine the voltage dependence of the current component blocked by ω-AgTx, the ramp currents recorded after toxin application were subtracted from control records (compare Fig. 12). Permeability estimates of the ω-AgTx–sensitive current (and the other components) as a function of voltage were constructed and fitted with Boltzmann functions. These plots are shown in Figure 13*B*. In contrast to previous reports (Regan et al., 1991), the ω-AgTx–sensitive, P-like current activated at relatively depolarized potentials ($V_h = 5.5$ mV, $V_c = 6.7$ mV); the voltage dependence of this component was virtually indistinguishable from that of the ω-CgTx–sensitive current ($V_h = 4.4$ mV, $V_c = 7.0$ mV). As shown above (Fig. 12*F*), the "resistant" and nifedipine-sensitive currents were similar in voltage dependence—activating at relatively negative membrane potentials (nifedipine: $V_h = -6.6$ mV, $V_c = 6.2$ mV; resistant: $V_h = -5.6$ mV, $V_c = 5.8$ mV). The inset shows the Boltzmann fits for each of these components on a normalized scale to allow a more ready comparison of voltage dependence. A statistical summary of the half-activation voltages (V_h) and the slope factor (V_c) is shown in Figure 13, *D* and *E*, respectively. An ANOVA analysis of the V_h values suggested that the differences between groups were significant ($p < 0.01$, Kruskal-Wallis ANOVA), whereas

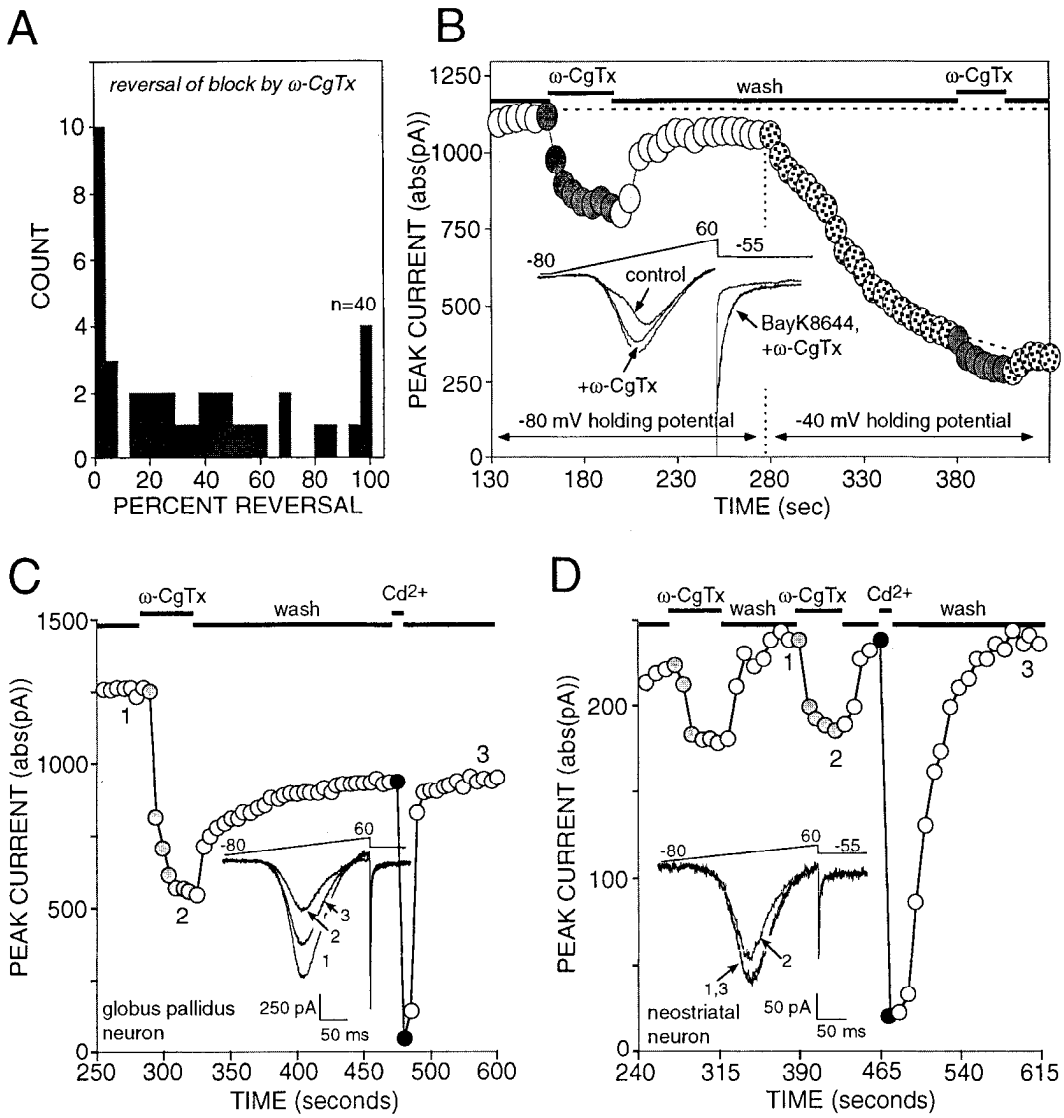

Figure 11. The ω-CgTx block is partially reversible in some neurons. *A*, Histogram of the percentage reversal of the block produced by ω-CgTx measured 2 min after the initiation of washing ($n = 40$). *B*, Time course of ω-CgTx block before and after changing the holding potential from −80 to −40 mV. Note that most current is recovered after washing. *Inset* shows currents from another cell in which ω-CgTx was applied after Bay K 8644 (1 μM). Note that although the peak current is reduced, the slow portion of the enhanced tail currents is not. *C*, Peak currents evoked by a voltage ramp in an acutely isolated globus pallidus neuron. The application of ω-CgTx (2 μM) produced a block that only partially reversed with washing in control solution (5 mM Ba^{2+}). *D*, Peak currents in a neostriatal neuron dissociated 20 min later were only transiently reduced with the same working solution of ω-CgTx.

the variation in V_c values was not ($p > 0.05$, Kruskal-Wallis ANOVA).

Single-cell aRNA amplification. Five distinct gene families have been cloned that give rise to Ca^{2+}-selective α1 subunits (Snutch et al., 1990; Mori et al., 1991; Tsien et al., 1991; Williams et al., 1992a,b; Snutch and Reiner, 1993; Soong et al., 1993). For the sake of simplicity, we will use the terminology introduced by Snutch et al. and refer to these gene families as classes A–E. Because the physiological analysis had shown that medium-sized cells expressed HVA currents, we attempted to determine whether these neurons expressed detectable quantities of mRNA thought to code for these channel classes. To do this, single medium-sized neostriatal neurons were recorded from and aspirated, and then cDNA was constructed from cytosolic polyadenylated mRNA. Double-stranded cDNA was then used to generate radiolabeled antisense RNA (aRNA) that was used to probe slot blots containing cDNAs for calcium channel mRNAs. cDNAs that selectively hybridized to mRNA of the rbA, rbB, and rbC classes were used (obtained from Dr. T. Snutch).

Twelve medium-sized neurons were recorded from and amplified. The Ca^{2+} channel expression profiles of all 12 were very similar. Shown in Figure 14*A* is an autoradiogram from a slot blot probed with aRNA from a neuron whose pharmacological profile is show to the right. In addition to a small ω-AgTx–sensitive current component, this neuron had a particularly large component that was irreversibly blocked by 2 μM ω-CgTx. Clearly detectable levels of class A and B mRNA were present in this neuron, in addition to mRNA for tyrosine kinase A (TRK, high-affinity NGF receptor), brain-derived neurotropic factor (BDNF), and neurofilament (NFIL). No specific labeling was observed to cDNA for the Bluescript (pBS) vector or glial fibrillary acidic

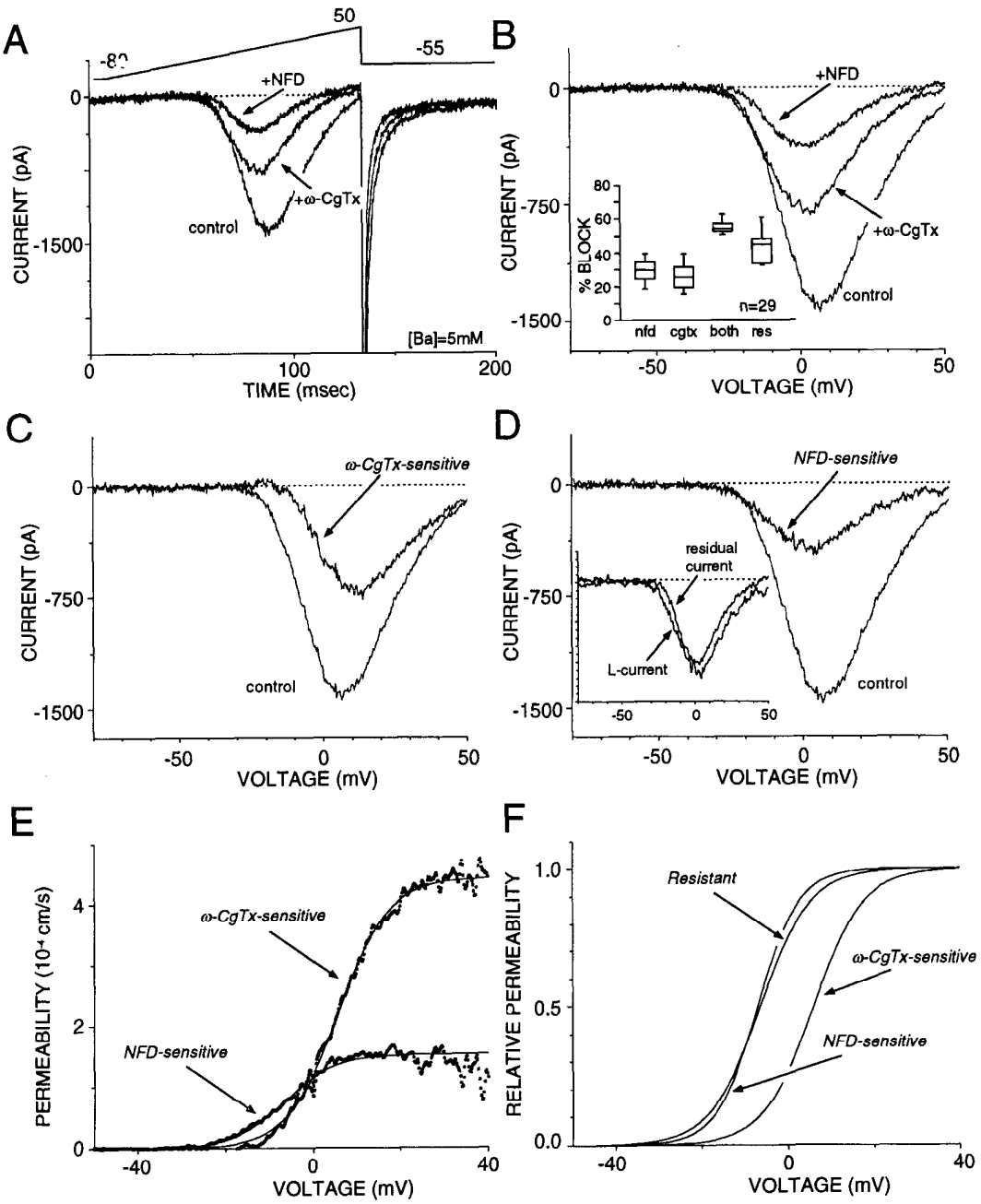

Figure 12. ω-CgTx and nifedipine affected distinct currents. *A*, Currents evoked by ramp depolarizations (stimulus shown at *top*) before (*control*) and after the addition of 1 μM ω-CgTx (+ω-*CgTx*) and 5 μM nifedipine in the maintained presence of ω-CgTx (+*NFD*). *Inset* shows a box plot of the percentage blocks in a sample of 20 cells. *B*, *I–V* plots from records in *A* after leak subtraction. Note that current designated as +NFD is the current resistant to both blockers. *C*, ω-CgTx–sensitive current is the current obtained after subtraction of the current recorded in the presence of the toxin (+ω-*CgTx*) from the current in control conditions (control). *D*, Nifedipine-sensitive current is also a subtraction of the current after from sensitive to ω-CgTx and nifedipine. *E*, Boltzmann fits to the permeability estimates of the nifedipine-sensitive and ω-CgTx–sensitive portions of the current. *F*, Normalized Boltzmann fits for the three components of the Ca^{2+}-current: ω-CgTx sensitive ("N"), nifedipine sensitive ("L"), and "resistant."

protein (GFAP). Surprisingly, no specific labeling was observed to the class C cDNA in this neuron, despite the presence of a nifedipine-sensitive current in every neuron studied. It is possible that the mRNA was present but at very low levels.

To determine whether the reversible block by ω-CgTx was correlated with the presence of a class B α1 subunit, amplifications were performed of cells with near or complete reversals (>80% reversal, $n = 4$). An autoradiogram from a neuron in which the ω-CgTx block was completely reversible (as in Fig. 11*D*) is shown in Figure 14*B*. As in neurons with irreversible block, a robust class B signal was seen. Similar patterns were observed in the other three neurons. It appears, therefore, that the reversibility of the ω-CgTx block is not correlated with the presence or absence of a class B gene product.

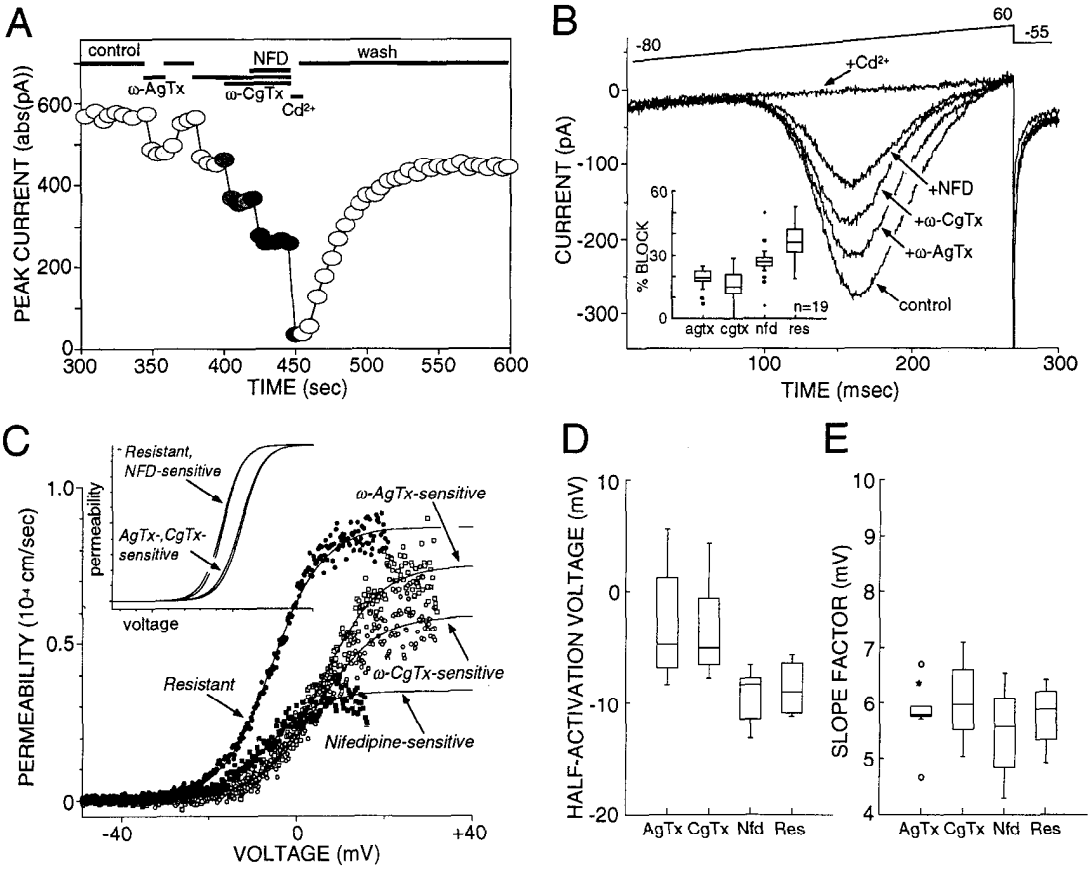

Figure 13. ω-Agatoxin IVA blocks a portion of the whole-cell Ca^{2+} current. *A*, Ramp currents evoked in control, in the presence of 100 nM ω-agatoxin IVA (*ω-AgTx*), of AgTx and 1 μM CgTx (*ω-CgTx*), of AgTx, CgTx and 5 μM nifedipine (*NFD*), and of 200 μM Cd^{2+} (*Cd^{2+}*). *B*, Representative current traces taken from the experiment depicted in *A*. *Inset* is a box plot of the percentage blocks derived from a sample of 19 cells (*single data points* are outliers). *C*, Permeability estimates of each current component based upon subtraction. Each set of data points was fitted with a Boltzmann function. *Inset* shows the Boltzmann fits plotted on a normalized ordinate; note that the AgTx- and CgTx-sensitive currents were very similar in voltage dependence, whereas the nifedipine-sensitive and-resistant currents were similar. *D*, Box plot summary of the half-activation voltages (V_h) for the AgTx-sensitive (n = 9), CgTx-sensitive (n = 6), nifedipine-sensitive (n = 7), and resistant (n = 4) currents. *E*, Box plot summary of the slope factors (V_c) for the same population.

Discussion

Ca currents in neostriatal neurons are heterogeneous

Our results show that Ca^{2+} currents in the somatic and proximal dendritic membrane of neostriatal neurons arise from a heterogeneous population of channels. In retrogradely identified medium spiny projection neurons, Ca^{2+} currents were exclusively of the HVA type.

To date, three types of HVA current have been identified in mammalian brain neurons: L-, N-, and P-type (Bean, 1989; Llinas et al., 1989; Hess, 1990; Tsien et al., 1991). Physiological studies have succeeded in separating these currents with pharmacological tools, but biophysical approaches have been less successful. More recent studies using combinations of N-, L-, and P-type current blockers have also reported a component of HVA current that is not blocked by these ligands (Mintz et al., 1992), suggesting that additional channel types are present in brain neurons (Hillyard et al., 1992).

Evidence for L-type currents

The evidence for the presence of L-type channels was biophysical and pharmacological. L-type currents typically activate rapidly and are relatively unaffected by holding at depolarized (~ −40 mV) membrane potentials. Neostriatal neurons clearly possessed currents with these characteristics. More importantly, the dihydropyridine antagonist nifedipine (1–10 μM) produced a reversible reduction in currents in every neuron studied (n > 50). In addition, the dihydropyridine agonist Bay K 8644 enhanced whole-cell currents and slowed tail current kinetics in a fashion similar to those seen in a number of cell types with L-type currents (Bean, 1989; Hess, 1990). Our failure to consistently detect class C mRNA, which is thought to code for the cardiac form of the L-type channel, may reflect a limitation in our ability to amplify low-abundance mRNAs sufficiently. Previous work has shown class C mRNA to be present in the striatum (Snutch et al., 1991). However, because L-type channels are restricted to somatic or proximal dendritic membrane and N-type channels are found throughout the cell (Westenbroek et al., 1992), the mRNA for L-type channels may be far less abundant than that for N-type (or P-type) channels. Further work with more sensitive methods, including aRNA-PCR (Eberwine et al., 1993), is needed on this point.

The biophysical and pharmacological data demonstrating the presence of L-type currents is consistent with the early report of Cherubini and Lanfumey (1987) that Bay K 8644 enhanced Ca^{2+} spikes in neostriatal neurons recorded in the slice prepa-

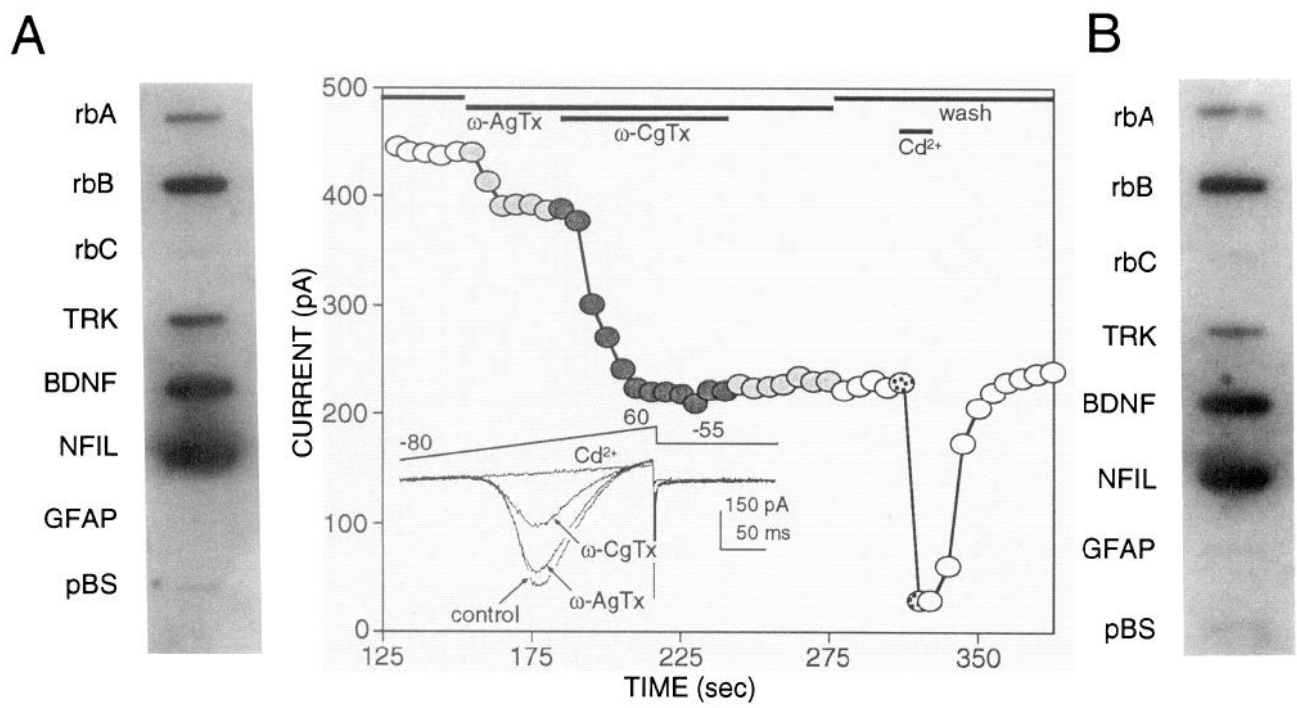

Figure 14. Single-cell aRNA amplification revealed the presence of rbA and rbB mRNA in pharmacologically characterized neurons. *A,* To the *left* is a slot blot derived from an acutely isolated neostriatal neuron (P29). Note that class A (*rbA*) and B (*rbB*) aRNA was detected, but class C (*rbC*) aRNA was not present (as judged by the similarity in signal level to that of the nonspecific labeling of the GFAP or pBS cDNA). To the *right* is a plot of peak current evoked by voltage ramps (shown in the *inset*) as a function of time and toxin application in the neuron used to construct the slot blot to the right. Note that the block by ω-CgTx was essentially irreversible. *B,* Slot blot derived from another neostriatal neuron in which the block by ω-CgTx was entirely reversible (as in Fig. 11*D*). *pBS,* Bluescript vector cDNA; *NFIL,* neurofilament cDNA; *GFAP,* glial fibrillary acidic protein cDNA; *BDNF,* brain-derived neurotrophic factor cDNA; *TRK,* tyrosine kinase A cDNA; CaM KII, Ca^{2+}/calmodulin-dependent protein kinase II cDNA.

ration. The presence of L-type, nitrendipine-sensitive currents in acutely isolated neostriatal neurons has also been shown by Hoehn et al. (1993). Although in agreement on their presence, we found a significantly larger fraction of the whole-cell current (20–40%) was sensitive to dihydropyridine antagonists. This discrepancy may reflect differences in abilities of nifedipine and nitrendipine to block striatal L-type channels. It is unlikely to have been the consequence of nifedipine block of N-type channels (Aosaki and Kasai, 1989) because (1) the blocks produced by nifedipine and ω-CgTx were largely additive and (2) the currents sensitive to each blocker differed in activation voltage dependence, kinetics, and sensitivity to holding potential.

The latter difference is of interest for another reason. In contrast to the ω-CgTx block, variation in the holding potential between −90 and −40 mV did not significantly alter the *absolute magnitude* of the nifedipine block at saturating concentration (5–10 μM). Although contrary to a commonly repeated interpretation, this finding is not inconsistent with the modified receptor model of dihydropyridine binding (Bean, 1984). Bean's results and those of others (e.g., Sanguinetti and Kass, 1986) show that the *affinity* of dihydropyridines for L-type channels appears to be voltage-dependent; however, at saturating concentrations (5–10 μM) these differences in affinity are of little consequence and L-channels, regardless of state, are blocked. In neurons possessing N-type currents that are inactivated by holding at depolarized potentials (Jones and Marks, 1989a), the percentage of the current that is blocked by saturating concentrations of dihydropyridines at depolarized potentials may be higher—not because the block of L-channels is voltage dependent, but because the proportion of *blockable* current has been changed by removing insensitive N-type channels. In our cells, the proportion of the current blocked by nifedipine was higher at a holding potential of −40 mV than at −80 mV only because of this fact.

Many of the other properties of the L-type current deduced from difference currents were similar to those described in other types of neurons. For example, both activation and deactivation kinetics were faster than N-type currents, as described previously (Matteson and Armstrong, 1986; Kostyuk and Shirokov, 1989; Regan et al., 1991; Kasai and Neher, 1992). One apparent difference was the relatively hyperpolarized threshold for activation of this component of the current (~−40 mV). In most descriptions, activation of L-type currents occurs at more depolarized potentials (Miller, 1987; Hosey and Lazdunski, 1988; Tsien et al., 1988). Some recent studies (Akaike et al., 1989; Aosaki and Kasai, 1989; Dichter and Zona, 1989; Mogul and Fox, 1991; Kasai and Neher, 1992), however, have found a voltage dependence similar to that in neostriatal neurons.

Evidence for N-type currents

In physiological studies, the only broadly accepted means of identifying N-type channels is by their sensitivity ω-CgTx GVIA (Tsien et al., 1988; Aosaki and Kasai, 1989; Carbone and Swandulla, 1989; Jones and Marks, 1989a). ω-CgTx (1–5 μM) typically blocked about 15–30% of the peak current evoked by voltage ramps. This proportion is similar to that reported by Hoehn et al. (1993) in acutely isolated neostriatal neurons and consistent with autoradiographic (Kerr et al., 1988; Takemura et al., 1989)

localization of these channels in the neostriatum. The significance of the proportion of the current that is of the N-type is not clear because N-type channels appear to be largely dendritic or in the presynaptic membrane (Westenbroek et al., 1992); as a result, their contribution to Ca^{2+} entry in an intact cell will be underestimated in our recordings from cells with truncated processes.

The N-type currents we did observe were similar in many respects to those described in other cells (Fox et al., 1987a; Jones and Marks, 1989a; Mogul and Fox, 1991; Regan et al., 1991; Artalejo et al., 1992; Mendelowitz and Kunze, 1992). As initially reported by Fox et al. (1987a,b), holding at depolarized membrane potentials (~−40 mV) significantly inactivated the ω-CgTx–sensitive current. Although several investigators have shown that the N-current cannot be unequivocally isolated by manipulations in holding potential (Aosaki and Kasai, 1989; Plummer et al., 1989; Mendelowitz and Kunze, 1992), voltage-dependent inactivation remains a important characteristic of this current (Jones and Marks, 1989b; Schroeder et al., 1990; Mogul and Fox, 1991). In addition, the N-type current activated and deactivated slowly, exhibiting kinetic characteristics very similar to those of N-type currents in other neurons (Kostyuk and Shirikov, 1989; Regan et al., 1991; Artalejo et al., 1992; Kasai and Neher, 1992; Mendelowitz and Kunze, 1992). The voltage dependence of activation was also very similar to what has previously been observed for N-type currents. What differed from previous descriptions was the *relative* voltage dependence of the current; that is, the N-type current activated at more depolarized potentials than the L-type currents. Although at variance with early reports derived from peripheral neurons (Fox et al., 1987a; Tsien et al., 1988, 1991), a similar pattern has been observed in several brain-derived cells (Aosaki and Kasai, 1989; Dichter and Zona, 1991; Regan et al., 1991; Kasai and Neher, 1992).

One difference with a number of previous reports (Feldman et al., 1987; McCleskey et al., 1987; Artalejo et al., 1992) was the finding that the block produced by ω-CgTx was often partially or completely reversed with washing. It is unlikely that the transience of the ω-CgTx effect was a consequence of a block of L-type channels (McCleskey et al., 1987; Aosaki and Kasai, 1989; Williams et al., 1992b) for at least three reasons. First, ω-CgTx did not affect the slow, Bay K 8644–enhanced L-type tail currents. Second, ω-CgTx did not occlude the block produced by the L-type current antagonist nifedipine. Lastly, the transiently blocked component of the current was sensitive to holding potential, unlike the DHP-sensitive component of the whole-cell current. Kinetic analysis of the on- and off-rates of the block revealed that only the off-rates appeared to be substantially altered. It is possible that enzyme treatment disrupted a portion of the extracellular face of the channel molecule and, in so doing, decreased the stability of the ω-CgTx–bound state. However, partial reversal of the ω-CgTx block of N-type channels have been described in cells not treated with enzyme (Plummer et al., 1989; Suprenant et al., 1990; Stack and Suprenant, 1991; Mynlieff and Beam, 1992). Plummer et al. (1989) hypothesized the existence of at least two populations of N-type channels with different binding affinities for ω-CgTx.

There is ample evidence for structural heterogeneity in ω-CgTx–sensitive channels. Class B mRNA is known to code for α1 subunits that are irreversibly blocked by ω-CgTx (Snutch et al., 1990; Tsien et al., 1991). These subunits are generally assumed to form the pore of N-type channels. In agreement with previous mRNA and protein localization studies (Dubel et al., 1992; Westenbroek et al., 1992), class B mRNA was found in every neostriatal neuron amplified. However, two other Ca^{2+} gene families are known to code for α1 subunits with ω-CgTx sensitivity—class D (Williams et al., 1992) and E (Ellinor et al., 1993) channels are reversibly blocked by micromolar ω-CgTx. Because of their sensitivity to dihydropyridines, it is unlikely that class D channels can account for the reversible ω-CgTx block in our neurons. Class E channels are also unlikely to be responsible because of their LVA-like properties. It is also possible that there is another, uncloned gene family coding for α1 subunits with reversible ω-CgTx binding. But, if the reversibly blocked current is coded for by a novel gene family, the abundance of class B mRNA in neurons with complete reversal of the ω-CgTx block must be explained. One possibility is that in these neurons, class B mRNA is not translated into protein. Another possibility is that translated protein is inserted in membrane lost during acute dissociation (i.e., distal dendrites or axonal terminals).

Evidence for P-type currents

In addition to N- and L-type currents, neostriatal neurons also express a P-type current, as judged by the sensitivity to ω-AgTx IVA. Although initially described in Purkinje neurons of the cerebellum, immunoreactivity for this channel type is found in a variety of other brain regions, including the striatum (Hillman et al., 1991). In most cells, 15–20% of the peak whole-cell current was blocked by ω-AgTx at concentrations reported to be saturating (100 nM; Mintz et al., 1992) for the native toxin. Higher concentrations (500 nM) of the synthetic toxin failed to block significantly more (>5%) of the peak current in a small sample of cells ($n = 10$). The reductions in peak current were not likely to have been a consequence of L-type channel block because ω-AgTx failed to reduce the slow, Bay K 8644 tail current. It was less clear whether ω-AgTx interacted with a portion of the current blocked by ω-CgTx. The median percentage of the peak current blocked by ω-CgTx was smaller after the application of ω-AgTx (16%) than ω-CgTx alone (25%). It is unclear whether this difference represents a true occlusion (and a channel blocked by both toxins) or sampling variation. Mintz et al. (1992) failed to find any indication that ω-AgTx at 100–200 nM blocked N-type channels in a variety of other central neurons. Further work is clearly needed on this point.

The molecular identity of the ω-AgTx–sensitive, P-like current remains to be firmly established. The correlation in individual neurons between the presence of class A mRNA and a P-like current is consistent with the hypothesis that class A mRNA codes for the α1 subunit of the P channel (Mori et al., 1991; Starr et al., 1991). Alternatively, class A mRNA may be responsible for the nominally resistant current in our cells. Preliminary experiments (Surmeier and Mermelstein, unpublished observations) have shown that a component of this "resistant" current is blocked by the *Conus magnus* toxin ω-CTx MVIIC (Hillyard et al., 1992), as are class A (BI) channels expressed in *Xenopus* oocytes (Sather et al., 1993).

Absence of LVA or T-type currents

Our inability to resolve a significant low-voltage-activated (LVA), T-like current in a large percentage of neostriatal neurons is at odds with a recent report by Hoehn et al. (1993). Based upon our earlier work with cultured embryonic striatal neurons (Bar-

gas et al., 1991) and preliminary work with acutely dissociated neurons from early postnatal animals (P2–P7), we expected to see this current in a larger percentage of cells than we did (<10%). The differences cannot readily be attributed to recording conditions or isolation procedure because we were able to see LVA currents, on occasion. It is also not likely that the use of cells with short dendritic processes precluded its detection because, in other cell types, LVA current appears to be largely in the soma and proximal dendrites (Llinas and Yarom, 1981; Llinas et al., 1984; Hernandez-Cruz and Pape, 1989). The most plausible explanation is that we have sampled different populations of neurons. Although 90–95% of neostriatal neurons are medium spiny projection neurons (Chang et al., 1982), these cells are heterogeneous in the expression of a variety of proteins (Reiner and Anderson, 1990; Gerfen, 1992). These differences may extend to Ca^{2+} channels. Another population of cells that could alter sample properties are interneurons. Although they account for only about 5–10% of the total neuronal population *in situ,* they may constitute a larger fraction of cells that survive acute dissociation and, hence, contribute disproportionately to a random sample of cells. The possibility that LVA currents are expressed in this smaller population is consistent with the relatively low levels of rbE mRNA seen in the neostriatum (Soong et al., 1993); expression of rbE mRNA gives rise to LVA-type Ca^{2+} currents. It is also consistent with recent work with striatal interneurons in slices by Kawaguchi (1993). These concerns were some of the motivation for using retrograde identification and single-cell expression profiling to be able to correlate phenotypic variables. In our limited sample of projection phenotypes (n = 23), LVA-type currents were not observed.

Another possible explanation for the differences in our results and those of Hoehn et al. (1992) is related to a seemingly small methodological difference. In our experiments, at every juncture in which neurons were ruptured (i.e., slicing and dissociation), the tissue was bathed in low-Ca^{2+} (100 μM), low-Cl^-, and high-Mg^{2+} (2–4 mM) solution to minimize Ca^{2+} loading and the release of neuromodulatory substances. If normally quiescent LVA currents are capable of being enhanced by a Ca^{2+}-dependent modulatory pathway (cf. Gray and Johnston, 1987), then we might not have detected their presence.

Despite these caveats, the absence of a substantial LVA current component in adult medium spiny neurons is consistent with their firing behavior in more intact preparations. In the slice, these neurons do not exhibit the properties normally associated with LVA currents, such as burst firing in response to depolarization from negative membrane potentials (Bargas et al., 1989). Also, medium spiny neurons do not have a prominent afterdepolarization or slowed spike-repolarizations even when spikes are evoked from hyperpolarized potentials (Pineda et al., 1992). These phenomena are commonly associated with the kinetically slower LVA current (McCobb and Beam, 1991). In contrast, these behaviors are seen in immature, early postnatal neostriatal neurons (Trent et al., 1992), as predicted from our earlier work in immature cells (Bargas et al., 1991b). This type of developmental elimination of LVA currents appears to be a characteristic of a great percentage of central neurons in descending motor pathways (i.e., pyramidal Betz neurons, spinal motoneurons; Llinas et al., 1988; Connors and Gutnick, 1990; Sayer et al., 1990; Mynlieff and Beam, 1992), whereas most ascending sensory neurons continue to manifest robust LVA currents (i.e., dorsal root ganglion neurons, dorsal horn spinal neurons, thalamic relay neurons, sensory cortex neurons, etc.; Llinas et al., 1988; Tsien et al., 1988, 1991, Hernandez-Cruz and Pape, 1989; Ryu and Randic, 1990; Sayer et al., 1990).

In summary, the Ca^{2+} currents in the somatic/proximal dendritic membrane of adult neostriatal neurons are attributable to HVA currents of the L-, N-, and P-types in addition to a fourth, pharmacologically undefined type of current. These currents have properties similar to those in other neurons except that the block of N-type current by ω-CgTx frequently reversed more rapidly than seen in most other cell types. In terms of voltage dependence, N- and P-type currents were indistinguishable, as were L-type and the resistant currents. mRNA expression profiling consistently found rbA and rbB mRNA in neostriatal neurons, in agreement with the hypothesis that these mRNAs code for the α1 subunit of P- and N-type channels, respectively.

References

Akaike N, Kostyuk PG, Osipchuk YV (1989) Dihydropyridine-sensitive low-threshold calcium channels in isolated rat hypothalamic neurones. J Physiol (Lond) 412:181–195.

Aosaki T, Kasai H (1989) Characterization of two kinds of high-voltage activated Ca-channel currents in chick sensory neurons. Pfluegers Arch 414:150–156.

Artalejo CR, Perlman RL, Fox AP (1992) ω-Conotoxin GVIA blockes a Ca^{2+} current in bovine chromaffin cells that is not of the "classic" N type. Neuron 8:85–95.

Augustine GJ, Charlton MP, Smith SJ (1987) Calcium action in synaptic transmitter release. Annu Rev Neurosci 10:633–693.

Bargas J, Galarraga E, Aceves J (1989) An early outward conductance modulates the firing latency and frequency of neostriatal neurons in the rat brain. Exp Brain Res 75:146–156.

Bargas J, Galarraga E, Aceves J (1991a) Dendritic activity on neostriatal neurons as inferred from somatic intracellular recordings. Brain Res 539:159–163.

Bargas J, Surmeier DJ, Kitai ST (1991b) High- and low-voltage activated calcium currents are expressed by rat neostriatal neurons. Brain Res 541:70–74.

Bean PB (1984) Nitrendipine block of cardiac calcium channels: high-affinity binding to the inactivated state. Proc Natl Acad Sci USA 81: 6388–6392.

Bean BP (1989) Classes of calcium channels in vertebrate cells. Annu Rev Physiol 51:367–384.

Beech DJ, Bernheim L, Hille B (1992) Pertussis toxin and voltage dependence distinguish multiple pathways modulating calcium channels of rat sympathetic neurons. Neuron 8:97–106.

Brehm P, Eckert R (1978) Calcium entry leads to inactivation of calcium channel in paramecium. Science 202:1203–1206.

Brown AM, Kunze DL, Yatani A (1984) The agonist effect of dihydropyridines on Ca channels. Nature 311:570–572.

Carbone E, Swandulla D (1989) Neuronal calcium channels: kinetics, blockade and modulation. Prog Biophys Mol Biol 54:31–58.

Chad J, Eckert R, Ewald D (1984) Kinetics of calcium-dependent inactivation of calcium current in voltage-clamped neurones of *Aplysia californica.* J Physiol (Lond) 347:279–300.

Chang HT, Wilson CJ, Kitai ST (1982) A Golgi study of rat neostriatal neurons: light microscopic analysis. J Comp Neurol 208:107–126.

Cherubini E, Lanfumey L (1987) An inward calcium current underlying regenerative calcium potentials in rat striatal neurons *in vitro* enhanced by Bay K 8644. Neuroscience 21:997–1005.

Connors BW, Gutnick MJ (1990) Intrinsic firing patterns of diverse neocortical neurons. Trends Neurosci 13:99–104.

Dichter MA, Zona C (1989) Calcium currents in cultured rat cortical neurons. Brain Res 492:219–229.

Eberwine J, Spencer C, Miyashiro K, Mackler S, Finnell R (1992a) Complementary DNA synthesis *in situ*: methods and applications. Methods Enzymol 216:80–100.

Eberwine J, Yeh H, Miyashiro K, Cao Y, Nair S, Finnell R, Zettel M, Coleman P (1992b) Analysis of gene expression in single live neurons. Proc Natl Acad Sci USA 89:3010–3014.

Feldman DH, Olivera BM, Yoshikami D (1987) Omega *Conus geographus* toxin: a peptide that blocks calcium channels. FEBS Lett 214: 295–300.

Fox AP, Nowycky MC, Tsien TW (1987a) Kinetic and pharmacolog-

ical properties distinguishing three types of calcium currents in chick sensory neurones. J Physiol (Lond) 394:149–172.
Fox AP, Nowycky MC, Tsien TW (1987b) Single-channel recordings of three types of calcium channels in chick sensory neurones. J Physiol (Lond) 394:173–200.
Galarraga E, Bargas J, Sierra A, Aceves J (1989) The role of calcium in the repetitive firing of neostriatal neurons. Exp Brain Res 75:157–168.
Galarraga E, Surmeier DJ, Kitai ST (1990) Quinolinate and kainate neurotoxicity in neostriatal cultures is potentiated by co-culturing with neocortical neurons. Brain Res 512:269–276.
Gerfen CR (1992) The neostriatal mosaic: multiple levels of compartmental organization. Trends Neurosci 15:133–139.
Giffin K, Solomon JS, Burkhalter A, Nerbonne J (1991) Differential expression of voltage-gated calcium channels in identified visual cortical neurons. Neuron 6:321–332.
Gray R, Johnston D (1987) Noradrenaline and β-adrenoreceptor agonists increase activity of voltage-dependent calcium channels in hippocampal neurons. Nature 327:620–622.
Hagiwara S, Ohmori H (1982) Studies of calcium channels in rat clonal pituitary cells with patch electrode voltage clamp. J Physiol (Lond) 331:231–252.
Hamill OP, Marty A, Neher E, Sakmann B, Sigworth FJ (1981) Improved patch-clamp techniques for high resolution current recording from cells and cell-free membrane patches. Pfluegers Arch 391:85–100.
Hernandez-Cruz A, Pape H-C (1989) Identification of two calcium currents in acutely dissociated neurons from the rat lateral geniculate nucleus. J Neurophysiol 61:1270–1283.
Herrington J, Lingle CJ (1992) Kinetic and pharmacological properties of low voltage-activated Ca^{2+} current in rat clonal (GH_3) pituitary cells. J Neurophysiol 68:213–232.
Hess P (1990) Calcium channels in vertebrate cells. Annu Rev Neurosci 13:337–356.
Hess P, Lansman JB, Nilius B, Tsien RW (1986) Calcium channel types in cardiac myocytes: modulation by dihydropyridines and beta-adrenergic stimulation. J Cardiovasc Pharmacol 8:S11–S21.
Hille B (1992) Ionic channels of excitable membranes. Sunderland, MA: Sinauer.
Hillman D, Chen S, Aung TT, Cherksey B, Sugimori M, Llinas RR (1991) Localization of P-type calcium channels in the central nervous system. Proc Natl Acad Sci USA 88:7076–7080.
Hillyard DR, Monje VD, Mintz IM, Bean BP, Nadasdi L, Ramachandran J, Miljanich G, Azimi-Zoonooz A, McIntosh JM, Cruz LJ, Imperial JS, Olivera BM (1992) A new *Conus* peptide ligand for mammalian presynaptic Ca^{2+} channels. Neuron 9:69–77.
Hirning LD, Fox AP, McCleskey EW, Olivera BM, Thayer SA, Miler RJ, Tsien RW (1988) Dominant role of N-type Ca^{2+} channels in evoked release of norepinephrine from sympathetic neurons. Science 239:57–61.
Hoehn K, Watson TWJ, MacVicar BA (1993) Multiple types of calcium channels in acutely isolated rat neostriatal neurons. J Neurosci 13:1244–1257.
Holliday J, Adams RJ, Sejnowski TJ, Spitzer NC (1991) Calcium-induced release of calcium regulates differentiation of cultured spinal neurons. Neuron 7:787–796.
Hosey MM, Lazdunski M (1988) Calcium channels: molecular pharmacology, structure and regulation. J Membr Biol 104:81–105.
Jones SW, Marks TN (1989a) Calcium currents in bullfrog sympathetic neurons. I. Activation kinetics and pharmacology. J Gen Physiol 94:151–167.
Jones SW, Marks TN (1989b) Calcium currents in bullfrog sympathetic neurons. II. Inactivation. J Gen Physiol 94:169–182.
Kaneda M, Akaike N (1989) The low-threshold Ca current in isolated amygdaloid neurons in the rat. Brain Res 497:187–190.
Kasai H, Neher E (1992) Dihydropyridine-sensitive and omega-conotoxin-sensitive calcium channels in a mammalian neuroblastoma–glioma cell line. J Physiol (Lond) 448:161–188.
Kass RS (1987) Voltage-dependent modulation of cardiac calcium channel current by optical isomers of Bay K 8644: implications for channel gating. Circ Res 61:I1–I5.
Kay AR, Wong RKS (1987) Calcium current activation kinetics in isolated pyramidal neurones of the CA1 region of the mature guinea-pig hippocampus. J Physiol (Lond) 392:603–616.
Kerr LM, Filloux F, Olivera BM, Jackson H, Wamsley JK (1988) Autoradiographic localization of calcium channels with [^{125}I] ω-conotoxin in rat brain. Eur J Pharmacol 146:181–183.
Kita H, Kita T, Kitai ST (1985) Active membrane properties of rat neostriatal neurons in an *in vitro* slice preparation. Exp Brain Res 60: 54–62.
Kostyuk PG (1989) Diversity of calcium ion channels in cellular membranes. Neuroscience 28:253–261.
Kostyuk PG, Shirokov RE (1989) Deactivation kinetics of different components of calcium inward current in the membrane of mice sensory neurones. J Physiol (Lond) 409:343–355.
Lancaster B, Nicoll RA, Perkel DJ (1991) Calcium activates two types of potassium channels in rat hippocampal neurons in culture. J Neurosci 11:23–30.
Llano I, Leresche N, Marty A (1991) Calcium entry increases the sensitivity of cerebellar Purkinje cells to applied GABA and decreases inhibitory synaptic currents. Neuron 6:565–574.
Llinas RR (1988) The intrinsic electrophysiological properties of mammalian neurons: insights into central nervous system function. Science 242:1654–1664.
Llinas R, Yarom Y (1981) Electrophysiology of mammalian inferior olivary neurons *in vitro*. Different types of voltage-dependent ionic conductances. J Physiol (Lond) 315:549–567.
Llinas R, Greenfield SA, Jahnsen H (1984) Electrophysiology of pars compacta cells in the *in vitro* substantia nigra—a possible mechanism for dendritic release. Brain Res 294:127–132.
Llinas R, Sugimori M, Lin JW, Cherksey B (1989) Blocking and isolation of a calcium channel from neurons in mammals and cephalopods utilizing a toxin fraction (FTX) from funnel-web spider poison. Proc Natl Acad Sci USA 86:1689–1693.
Malecot CO, Feindt P, Trautwein W (1988) Intracellular *N*-methyl-D-glucamine modifies the kinetics and voltage-dependence of the calcium current in guinea pig ventricular heart cells. Pfluegers Arch 411: 235–242.
Matteson DR, Armstrong CM (1986) Properties of two types of calcium channels in clonal pituitary cells. J Gen Physiol 87:161–182.
McCleskey EW, Fox AP, Feldman DH, Cruz LJ, Olivera BM, Tsien RW, Yoshikami D (1987) ω-Conotoxin: direct and persistent blockade of specific types of calcium channels in neurons but not muscle. Proc Natl Acad Sci USA 84:4327–4331.
Mendelowitz D, Kunze DL (1992) Characterization of calcium currents in aortic baroreceptor neurons. J Neurophysiol 68:509–517.
Miller RJ (1987) Multiple calcium channels and neuronal function. Science 235:46–52.
Miller RJ (1988) Calcium signaling in neurons. Trends Neurosci 11: 415–424.
Mintz IM, Adams ME, Bean BP (1992) P-type calcium channels in rat central and peripheral neurons. Neuron 9:85–95.
Mogul DJ, Fox AP (1991) Evidence for multiple types of Ca^{2+} channels in acutely isolated hippocampal CA3 neurones of the guinea-pig. J Physiol (Lond) 433:259–281.
Muller W, Connor JA (1991) Cholinergic input uncouples Ca^{2+} changes from K^+ conductance activation and amplifies intradendritic Ca^{2+} changes in hippocampal neurons. Neuron 6:901–905.
Murphy TH, Worley PF, Baraban JM (1991) L-type voltage-sensitive calcium channels mediate synaptic activation of immediate early genes. Neuron 7:625–635.
Mynlieff M, Beam KG (1992) Characterization of voltage-dependent calcium currents in mouse motoneurons. J Neurophysiol 68:85–92.
Nakanishi H, Kita H, Kitai ST (1987) Intracellular study of rat substantia nigra pars reticulata neurons in an *in vitro* slice preparation: electrical membrane properties and response characteristics to subthalamic stimulation. Brain Res 437:45–55.
Narahashi T, Tsunoo A, Yoshii M (1987) Characterization of two types of calcium channels in mouse neuroblastoma cells. J Physiol (Lond) 383:231–249.
Pare D, Curro'Dossi R, Steriade M (1990) Neuronal basis of the parkinsonian resting tremor: a hypothesis and its implications for treatment. Neuroscience 35:217–226.
Park MR, Lighthall JW, Kitai ST (1980) Medium spiny neuron projection from the rat striatum: an intracellular horseradish peroxidase study. Brain Res 194:359–369.
Pineda JC, Galarraga E, Bargas J, Cristancho M, Aceves J (1992) Charybdotoxin and apamin sensitivity of the calcium-dependent repolarization and the afterhyperpolarization in neostriatal neurons. J Neurophysiol 68:287–294.

Plummer MR, Logothetis DE (1989) Elementary properties and pharmacological sensitivities of calcium channels in mammalian peripheral neurons. Neuron 2:1453–1463.

Rassmussen H, Barrett PQ (1984) Calcium messenger system: an integrated view. Physiol Rev 64:938–984.

Regan LJ (1991) Voltage-dependent calcium currents in purkinge cells from rat cerebellar vermis. J Neurosci 11:2259–2269.

Regan LJ, Sah DWY, Bean B (1991) Ca^{2+}-channels in rat central and peripheral neurons: high-threshold current resistant to dihydropyridine blockers and omega-conotoxin. Neuron 6:269–280.

Reiner A, Anderson KD (1990) The patterns of neurotransmitter and neuropeptide co-occurrence among striatal projection neurons: conclusions based on recent findings. Brain Res Rev 15:251–265.

Rose WC, Balke CW, Wier WG, Marban E (1992) Macroscopic and unitary properties of physiological ion flux through L-type Ca^{2+} channels in guinea-pig heart cells. J Physiol (Lond) 456:267–284.

Ryu PD, Randic M (1990) Low- and high-voltage-activated calcium currents in rat spinal dorsal horn neurons. J Neurophysiol 63:273–285.

Sanguinetti MC, Krafte DS, Kass RS (1986) Voltage-dependent modulation of Ca channel current in heart cells by Bay K 8644. J Gen Physiol 88:369–392.

Sather WA, Tanabe T, Zhang J-F, Mori Y, Adams ME, Tsien RW (1993) Distinctive biophysical and pharmacological properties of class A (BI) calcium channel $\alpha 1$ subunits. Neuron 11:291–303.

Sayer RJ, Schwindt PC, Crill WE (1990) High- and low-threshold calcium currents in neurons acutely isolated from rat sensorimotor cortex. Neurosci Lett

Schroeder JE, Fischbach PS, Mamo M, McCleskey EW (1990) Two components of high-threshold Ca current inactivate by different mechanisms. Neuron 5:445–452.

Snutch TP, Reiner PB (1992) Ca^{2+} channels: diversity of form and function. Curr Opin Neurobiol 2:247–253.

Snutch TP, Leonard JP, Gilbert MM, Lester HA, Davidson N (1990) Rat brain expresses a heterogeneous family of calcium channels. Proc Natl Acad Sci USA 87:3391–3395.

Snutch TP, Tomlinson WJ, Leonard JP, Gilbert MM (1991) Distinct calcium channels are generated by alternative splicing and are differentially expressed in the mammalian CNS. Neuron 7:45–57.

Soong TW, Stea A, Hodson CD, Dubel SJ, Vincent SR, Snutch TP (1993) Structure and functional expression of a member of the low-voltage-activated calcium channel family. Science 260:1133–1136.

Stack J, Surprenant AM (1991) Dopamine actions on calcium currents, potassium currents and hormone release in rat melanotrophs. J Physiol (Lond) 439:37–58.

Surmeier DJ, Stefani A, Foehring R, Kitai ST (1991) Developmental expression of a slowly-inactivating voltage dependent potassium current in rat neostriatal neurons. Neurosci Lett 122:41–46.

Surmeier DJ, Eberwine J, Wilson CJ, Stefani A, Kitai ST (1992) Dopamine receptor subtypes co-localize in rat striatonigral neurons. Proc Natl Acad Sci USA 89:10178–10182.

Surmeier DJ, Seno T, Kitai ST (1994) Acutely-isolated globus pallidus neurons express four types of high-voltage activated calcium current. J Neurophysiol, in press.

Surprenant A, Shen KZ, North RA, Tatsumi H (1990) Inhibition of calcium currents by noradrenaline, somatostatin and opioids in guinea-pig submucosal neurones. J Physiol (Lond) 431:585–608.

Swandulla D, Armstrong CM (1989) Calcium channel block by cadmium in chicken sensory neurons. Proc Natl Acad Sci USA 86:1736–1740.

Takahashi K, Wakamori M, Akaike N (1989) Hippocampal CA1 pyramidal cells of rats have four voltage-dependent calcium conductances. Neurosci Lett 104:229–234.

Takemura M, Kiyama H, Fukui H, Tohyama M, Wada H (1988) Autoradiographic visualization in rat brain of receptors for ω-conotoxin GIVA, a newly discovered calcium antagonist. Brain Res 451: 386–389.

Trent F, Xu ZC, Wilson CJ, Tepper JM (1992) A cadmium-sensitive voltage-dependent conductance is transiently expressed during development in rat neostriatal neurons. Soc Neurosci Abstr 18:697.

Tsien RW, Lipscombe D, Madison DV, Bley KR, Fox AP (1988) Multiple types of neuronal calcium channels and selective modulation. Trends Neurosci 11:431–439.

Tsien RW, Ellinor PT, Horne WA (1991) Molecular diversity of voltage-dependent Ca^{2+} channels. Trends Pharmacol Sci 12:349–354.

Tukey JW (1977) Exploratory data analysis. Menlo Park, CA: Addison-Wesley.

Usowicz MM, Sugimori M, Cherskey B, Llinas R (1992) P-type calcium channels in the somata and dendrites of adult cerebellar Purkinje cells. Neuron 9:1185–1199.

VanGelder RN, von Zastrow ME, Yool A, Dement WC, Barchas JD, Eberwine JH (1990) Amplified RNA synthesized from limited quantities of heterogeneous cDNA. Proc Natl Acad Sci USA 87:1663–1667.

Westenbroek RE, Hell JW, Warner C, Dubel SJ, Snutch TP, Catterall WA (1992) Biochemical properties and subcellular distribution of an N-type calcium channel $\alpha 1$ subunit. Neuron 9:1099–1115.

Williams ME, Brust PF, Feldman KH, Patthi S, Simerson S, Maroufi A, McCue AF, Velicelebi G, Ellis SB, Harpold MM (1992a) Structure and functional expression of an omega-conotoxin-sensitive human N-type calcium channel. Science 257:389–395.

Williams ME, Feldman KH, McCue AF, Brenner R, Velicelebi G, Ellis SB, Harpold MM (1992b) Structure and functional expression of $\alpha 1$ and $\alpha 2$ and beta subunits of a novel human neuronal calcium channel subtype. Neuron 8:71–84.

Wilson CJ, Chang HT, Kitai ST (1983) Disfacilitation and long-lasting inhibition of neostriatal neurons in the rat. Exp Brain Res 51:227–235.